Lindblad Equation, Symmetries, and Instabilities in Driven-Dissipative Systems

Master's Thesis

Submitted to the Faculty of Mathematics, Computer Science and Natural Sciences at RWTH Aachen University

presented by

Steven Kim

under the supervision of

Prof. Dr. Fabian Hassler

and

Prof. Dr. Markus Müller

JARA-Institute for Quantum Information

05/2023

Abstract

This thesis deals with driven-dissipative systems that can be described by a Lindblad master equation. In particular, we analyze parametrically driven oscillators that exhibit an instability when the driving strength exceeds the damping. In this critical regime, both fluctuations and nonlinearities have to be included for an accurate description of the system. For the degenerate parametric oscillator, it has been shown that the long-time dynamics can be described by a universal Liouvillian. This makes the efficient calculation of observables, such as the photon current, possible. To determine the long-time dynamics, we provide a method to solve the Lindblad equation, which makes the separation of timescales possible. This is used to derive the effective model for the non-degenerate parametric oscillator, and we analyze the resulting statistics of radiation. Additionally, we discuss how symmetries of the Lindblad equation are described.

Contents

List of Figures

Chapter 1

Introduction and chapter overview

This thesis deals with driven-dissipative systems that can be described by a Lindblad master equation. In particular, we treat parametrically driven oscillators. They are a prime example for systems with an instability, when the driving strength exceeds the damping. For the classical system, self-sustained oscillations are possible above threshold, while the system reaches the state of rest below threshold. In the quantum regime, a parametric drive makes the amplification of quantum fluctuations already below threshold possible. This results in a finite number of photons leaking out of the cavity. The radiation is characterized by the emission of a photon pair enabled by the prior absorption of a photon with twice the frequency, also known as parametric down-conversion. This can be e.g. used to create squeezed states of light [1] or entangled pairs of photons [2].

For this system, the transition at the instability threshold is also called pitchfork bifurcation. At the transition, the state of rest becomes unstable and two new stable fixed points emerge. Other systems also realize the bifurcation, such as the Dicke [3] and lasing [4] transitions. It has been shown that systems with such a bifurcation are part of a universality class in Ref. [5]. There, the counting statistics of photons, or rather quantized frequency excitations, below threshold have been derived. Without regard of the nonlinearity, all cumulants of the photon current diverge as the threshold is approached. Besides fluctuations, also nonlinearities have to be included in this critical regime. They cure the divergence and the system reaches a coherent state. This results in Poissonian statistics that match the classical expectation. The link between the two regimes was missing, until Ref. [6] connected them. There, a universal model of the relevant slow dynamics in the close vicinity of the threshold has been derived. The resulting photon statistics show a good agreement with the full system.

The systems discussed in Refs. [5, 6] share a common feature, the pitchfork bifurcation. This bifurcation is not present for the non-degenerate parametric

oscillator. Nevertheless, it is still part of the universality class in Ref. [5]. Therefore, the counting statistics of the non-degenerate and degenerate parametric oscillator are equivalent. However, in the non-degenerate case, it is possible to achieve phase-insensitive amplification. This is qualitative different than the degenerate case where phase-sensitive amplification is achieved. Therefore, we study the non-degenerate parametric oscillator in the critical regime and derive an effective model for this system. We focus on the resulting counting statistics and compare to the degenerate case as well as the classical expectation. As the focus is lied upon the radiation, the methods and resulting models provide a good starting point for a variety of follow-up work to further analyze the dynamics of both the non-degenerate and degenerate parametric oscillator.

To obtain the effective models, we start with the general description of a driven-dissipative system that interacts with its (Markovian) environment, e.g. through the emission and absorption of photons, in Ch. 2. Such systems can be described by a Lindblad master equation, that can be compactly expressed by a Liouvillian $\mathcal{L}$, which determines the time evolution of the system. For the determination of the time evolution operator $\exp(\mathcal{L}t)$ it is necessary to determine the eigenvalues and therefore the diagonalized form of the Liouvillian. But the diagonalization is non-trivial for multiple reasons, e.g. the already infinitely large Hilbert space of a single boson. Therefore, we provide a method to solve this task that makes use of symplectic transformations, which take the bosonic structure into account. The method can also be used to obtain the generating function that contains the information about the cumulants of observables, such as the photon current.

The introduced framework can be used to describe symmetries of the Lindblad equation, which is the topic of Ch. 3. We begin by considering the hermiticity of the density matrix, although it is not a symmetry in the conventional sense. It rather puts constraints on the Liouvillian and also provides a useful tool for the diagonalization. We then describe how unitary symmetries of the Hamiltonian can be extended to symmetries of the full Liouvillian. We conclude by a discussion about $\mathcal{PT}$-symmetries, which characterizes systems with balanced gain and loss.

Chapter 4 reviews Ref. [6] which investigates the degenerate parametric oscillator in the critical regime. We explain how the introduced formalism of this work can be used to obtain the universal model by a separation of timescales. Additional results are provided as well. The methods are then used in Ch. 5, where the non-degenerate case is approached and a universal Liouvillian is derived. The degenerate and non-degenerate parametric are compared, and an efficient numerical evaluation of the Liouvillians is demonstrated.

Chapter 2

Solving the Lindblad master equation

In a realistic setting, quantum systems interact with their environment, e.g. via emission or absorption of photons. For Markovian environments, the equation governing the dynamics of the system is given by a Lindblad master equation which reads

$$\dot{\rho} = -i[\mathcal{H}, \rho] + \sum_{\mu} \Big[\mathcal{J}_\mu \rho \mathcal{J}_\mu^\dagger - \frac{1}{2}(\mathcal{J}_\mu^\dagger \mathcal{J}_\mu \rho + \rho \mathcal{J}_\mu^\dagger \mathcal{J}_\mu) \Big]. \tag{2.1}$$

The first part of the equation equals the von Neumann equation with the Hamiltonian H that describes the closed system in a rotating frame. It contains the unitary time evolution of the system. The second part describes the coupling to the bath and contains the dissipative, non-unitary dynamics. The Lindblad operators $\mathcal{J}_\mu$ resemble the dissipation processes. The equation can be expressed by a Liouvillian superoperator[1] $\mathcal{L}$ with $\dot{\rho} = \mathcal{L}\rho$. The solution of this, is then given by the time evolution operator $\exp(\mathcal{L}t)$. To understand the dynamics of the system, the eigenvalues λ of the Liouvillian are needed. In particular, they are of interest for dissipative phase transitions when $\mathrm{Re}(\lambda) \to 0$ [7]. They also allow to identify instabilities where $\mathrm{Re}(\lambda) > 0$. There, the dynamics diverge exponentially. But obtaining the spectrum is a non-trivial task for multiple reasons. For example, the Hilbert space of a single boson is already infinite dimensional, which makes the standard matrix diagonalization impossible. Furthermore, we have to consider the underlying bosonic structure of the problem that is encoded in the commutation relations. To circumvent these issues, a method called 'third quantization' has been first developed for fermions in Ref. [8] and has later been extended to the case of bosons [9]. The method has also been used to solve bosons on a lattice [10] and also nonlinear systems by employing weak symmetries [11]. Recently, the connection to the Keldysh path-integral formulation of open systems has been pointed out [12, 13]. Also, the method can be used to separate fast and slow timescales. This makes the reduction to the relevant slow dynamics for long times possible, which has been done in Ref. [6] and will also be discussed below.

[1] Sometimes also *Liouvillian*, *Liouville superoperator*, or *Lindbladian*.

In this chapter, we propose an alternative method to 'third quantize' a quadratic bosonic Lindblad master equation using symplectic transformations. The results of this and the following chapter are discussed in a paper in Ref. [14].

2.1 Symplectic diagonalization of complex symmetric matrices

We will map the problems mentioned above onto the diagonalization of complex matrices using symplectic transformations. In the applications, the symplectic form arises due to the bosonic structure of the problem that is encoded in the commutation relations. We prepare the main theorem by two lemmas.

The first lemma is a restatement of the diagonalization of a complex matrix:

Lemma 1. *Given the standard symplectic form ($J^T = J^{-1} = -J$)*

$$J = \begin{pmatrix} 0 & I_n \\ -I_n & 0 \end{pmatrix}, \tag{2.2}$$

where I_n is the identity matrix of size n, a symmetric matrix $L \in \mathbb{C}^{2n\times 2n}$, $L = L^T$, with $J^{-1}L$ diagonalizable, can be brought into the normal form

$$PLQ = \begin{pmatrix} 0 & \Lambda \\ \Lambda & 0 \end{pmatrix}; \tag{2.3}$$

where Λ is a diagonal matrix with entries $\lambda_1, \ldots, \lambda_n$ and $P, Q \in \mathrm{GL}(2n, \mathbb{C})$ are (invertible) transition matrices with

$$PJQ = J\,. \tag{2.4}$$

Proof. The matrix $A = J^{-1}L$ can be diagonalized by a transition matrix Q and a diagonal matrix D with $Q^{-1}AQ = D$. Note that $A = -J^{-1}A^TJ$ such that A is similar to $-A^T$. Thus, the eigenvalues of A come in pairs $\pm\lambda_i$. Due to this, we can choose

$$D = \begin{pmatrix} -\Lambda & 0 \\ 0 & \Lambda \end{pmatrix}. \tag{2.5}$$

With $P = JQ^{-1}J^{-1}$, we have $J^{-1}PLQ = D$ and the result follows by

$$JD = \begin{pmatrix} 0 & \Lambda \\ \Lambda & 0 \end{pmatrix}. \tag{2.6}$$

□

Remark 1. The column vectors $\boldsymbol{q}_i$ of Q together with the eigenvalues λ_i can be obtained by solving the generalized eigenvalue problem

$$L\boldsymbol{q}_i = \lambda_i J\boldsymbol{q}_i\,. \tag{2.7}$$

Remark 2. If $A = J^{-1}L$ is not diagonalizable, the theorem can be adjusted such that Λ involves Jordan blocks and

$$D = \begin{pmatrix} -\Lambda & 0 \\ 0 & \Lambda^T \end{pmatrix}. \tag{2.8}$$

We give an example of this case below.

The following technical lemma will be the central ingredient of the theorem:

Lemma 2. *Given an invertible transition matrix $T \in \mathrm{GL}(2n, \mathbb{C})$ and an arbitrary matrix $A \in \mathbb{C}^{2n\times 2n}$ with*

$$A = T^T A T^{-1}, \tag{2.9}$$

we can find $B \in \mathrm{GL}(2n, \mathbb{C})$ such that $B^2 = T$ (B is a 'square root' of T) and

$$A = B^T A B^{-1}. \tag{2.10}$$

Proof. From (2.9), it follows by iteration that

$$A = (T^k)^T A (T^k)^{-1}, \qquad k \in \mathbb{N} \tag{2.11}$$

and also that $A = p(T)^T A\, p(T)^{-1}$ for an arbitrary polynomial $p(x)$. The function $f(x) = \sqrt{x}$ evaluated on T only depends on the value on the spectrum of T, see [15] for details. As the spectrum of T does not involve 0, we can choose a single-valued branch of $f(x)$ and find a polynomial $p_f(x)$ that has the same value as $f(x)$ on the spectrum of T. The matrix $B = p_f(T)$ fulfills the requirements $B^2 = T$ and Eq. (2.10) of the lemma. □

Now, we have prepared the necessary tools to proof our main theorem.

Theorem 1. *Given the conditions of lemma 1, the symmetric matrix L can be brought into the normal form*

$$S^T L S = \begin{pmatrix} 0 & \Lambda \\ \Lambda & 0 \end{pmatrix} \tag{2.12}$$

by a symplectic transition matrix S fulfilling

$$S^T J S = J. \tag{2.13}$$

Proof. With lemma 1, the symmetry of L, and the skew-symmetry of J, it follows that

$$PLQ = Q^T L P^T = \begin{pmatrix} 0 & \Lambda \\ \Lambda & 0 \end{pmatrix} \qquad \text{and} \qquad PJQ = Q^T J P^T = J. \tag{2.14}$$

This implies that

$$L = T^T L T^{-1} \qquad \text{and} \qquad J = T^T J T^{-1}, \tag{2.15}$$

where $T = Q(P^{-1})^T = QP^{-T}$. Using lemma 2, we obtain B with $B^2 = T$ and B fulfilling the properties of (2.10). Setting $S = B^{-1}Q$, we obtain (X is either L or J)

$$S^T X S = Q^T B^{-T} X B^{-1} Q \overset{(2.15)}{=} Q^T (B^{-T})^2 X Q = Q^T T^{-T} X Q = PXQ\,. \quad (2.16)$$

The result follows from comparing $S^T L S = PLQ$ in Eq. (2.3) and $S^T J S = PJQ$ in Eq. (2.4).

□

Remark 3. The normal form is unique up to reordering of the λ_i or replacing λ_i by its partner $-\lambda_i$. In particular, for each $i \leq n$, the normal form is invariant under the exchange $\boldsymbol{s}_i \mapsto -\boldsymbol{s}_{i+n}$ and $\boldsymbol{s}_{i+n} \mapsto \boldsymbol{s}_i$ of the i-th and $(i+n)$-th column of S while inverting the sign of $\lambda_i \mapsto -\lambda_i$. In the application for open systems, the sign of λ_i will determine the stability of the system. We will discuss how to fix the sign ambiguity for the elements of Λ below.

Remark 4. For an alternative proof using symplectic geometry induced by the form $\omega(\boldsymbol{x}, \boldsymbol{y}) = \boldsymbol{x}^T J \boldsymbol{y}$, see [16].

Remark 5. Note that the presented theorem is different from the better-known Williamson's theorem for the diagonalization of a real, symmetric, positive matrix with a symplectic transition matrix, see e.g. [17].

2.2 Solving a bosonic Lindblad master equation

Now, we have gathered the tool to 'third quantize' the Liouvillian $\mathcal{L}$. In this section, we show how to map the task of solving the Liouvillian to the symplectic eigenvalue problem from the previous section.

2.2.1 Superoperator formalism and non-Hermitian Hamiltonian

For exact solvability, we assume that the Hamiltonian is at most quadratic in bosonic ladder operators $a_i, i = 1, \ldots, m$ with m being the number of different modes and that the bath operators are linear in ladder operators. This means that

$$\mathcal{H} = \sum_{i,j}\left[a_i^\dagger h_{ij} a_j + \tfrac{1}{2} a_i \Delta_{ij} a_j + \tfrac{1}{2} a_i^\dagger (\Delta^\dagger)_{ij} a_j^\dagger\right] + \sum_i \left(\alpha_i^* a_i + \alpha_i a_i^\dagger\right), \quad (2.17)$$

$$\mathcal{J}_\mu = \sum_i \left(v_{\mu,i} a_i + w_{\mu,i} a_i^\dagger\right) + l_\mu. \quad (2.18)$$

The matrix $h \in \mathbb{C}^{m\times m}$ is Hermitian, and it is possible to choose $\Delta \in \mathbb{C}^{m\times m}$ as a symmetric matrix. The vectors $\boldsymbol{v}_\mu, \boldsymbol{w}_\mu \in \mathbb{C}^m$ describe the interaction with the environment. Emission is described by the first, while the latter relates to absorption. The coherent drive $\alpha_i \in \mathbb{C}$ and the parameters $l_\mu \in \mathbb{C}$ couple linearly to the bosonic ladder operators and thus displace the vacuum, see below.

Since the operators in the Lindblad equation act on both sides of the density matrix, we introduce a superoperator formalism. We define a set of superoperators by $\mathcal{O}_c = (\mathcal{O}_+ + \mathcal{O}_-)/\sqrt{2}$ and $\mathcal{O}_q = (\mathcal{O}_+ - \mathcal{O}_-)/\sqrt{2}$ where $\mathcal{O}_+\rho = \mathcal{O}\rho$

and $\mathcal{O}_-\rho = \rho\mathcal{O}$. The subscripts 'c' and 'q', denoting 'classical' and 'quantum', come from the language used in the Keldysh path-integral formalism [18]. The commutation relations are $[a_{c,i}, a^\dagger_{q,j}] = [a_{q,i}, a^\dagger_{c,j}] = \delta_{ij}$. The remaining commutators vanish. Using this definition and defining the basis $\boldsymbol{b} = (\boldsymbol{b}_c, \boldsymbol{b}_q)^T = (\boldsymbol{a}_c, \boldsymbol{a}_c^\dagger, \boldsymbol{a}_q^\dagger, -\boldsymbol{a}_q)^T$, we can express the Liouvillian by a complex symmetric matrix $L \in \mathbb{C}^{2n\times 2n}$ with $n = 2m$. The Liouvillian reads $\mathcal{L} = \frac{1}{2}\boldsymbol{b}^T L \boldsymbol{b} + \boldsymbol{\eta}\cdot\boldsymbol{b}_q + L_0$ with

$$L = \begin{pmatrix} 0 & -iH_{\text{eff}}^T Z \\ -iZH_{\text{eff}} & N \end{pmatrix}, \tag{2.19}$$

$$\boldsymbol{\eta} = \begin{pmatrix} \boldsymbol{z} \\ \boldsymbol{z}^* \end{pmatrix}, \quad \boldsymbol{z} = -i\boldsymbol{\alpha} + \tfrac{1}{2}\textstyle\sum_\mu \left(l_\mu^* \boldsymbol{w}_\mu - l_\mu \boldsymbol{v}_\mu^*\right) \in \mathbb{C}^m, \tag{2.20}$$

and $L_0 = \frac{1}{2}\operatorname{Tr}(V - W)$. The 'dissipation matrices' V, W, and $U \in \mathbb{C}^{m\times m}$ are defined by the sum of dyadic products

$$V = V^\dagger = \sum_\mu \boldsymbol{v}_\mu \boldsymbol{v}_\mu^\dagger, \quad W = W^\dagger = \sum_\mu \boldsymbol{w}_\mu \boldsymbol{w}_\mu^\dagger, \quad U = -\sum_\mu \boldsymbol{v}_\mu \boldsymbol{w}_\mu^\dagger. \tag{2.21}$$

We continue to analyze the block structure of L. Note that the upper left block of the matrix equals zero. This implies the trace preservation of the Lindblad equation. This block would connect the 'c'-operators to each other. Since terms like this do not appear, there is always at least on 'q'-operator in each term of the Liouvillian. This relates to the trace preservation by $\operatorname{Tr}(\mathcal{O}_q\rho) = \operatorname{Tr}(\mathcal{O}\rho - \rho\mathcal{O}) = 0$. Below, we show that the trace preservation is the key ingredient that makes the diagonalization of the Liouvillian possible. The matrix $N \in \mathbb{C}^{2m\times 2m}$ is given by

$$N = \frac{1}{2}\begin{pmatrix} U^\dagger + U^* & W + V^* \\ W^* + V & U^T + U \end{pmatrix}. \tag{2.22}$$

It only depends on the dissipation matrices and resembles the noise in the system [13]. Due to the 0 in the upper left block of the Liouvillian, N and therefore the noise does not influence the eigenvalues λ of the system. In contrast, the effective Hamiltonian H_{eff} on the off-diagonals encodes the dynamics of the system. Here, we have split the matrix

$$Z = \begin{pmatrix} I_m & 0 \\ 0 & -I_m \end{pmatrix} \tag{2.23}$$

from the effective Hamiltonian. It encodes the bosonic commutation relations $[a_i, a_j^\dagger] = \delta_{ij}$ [19]. Then, H_{eff} can be written as

$$H_{\text{eff}} = \begin{pmatrix} h + \frac{i}{2}(W - V^*) & \Delta^* - \frac{i}{2}(U^\dagger - U^*) \\ \Delta + \frac{i}{2}(U^T - U) & h^* - \frac{i}{2}(W^* - V) \end{pmatrix}. \tag{2.24}$$

It can be decomposed into two parts by $H_{\text{eff}} = H + i\Gamma$ where H and Γ are both Hermitian. The first part, H, is the Hamiltonian that describes the closed system given by $\mathcal{H} = \frac{1}{2}\boldsymbol{b}'^\dagger H \boldsymbol{b}'$ with $\boldsymbol{b}' = (\boldsymbol{a}, \boldsymbol{a}^\dagger)^T$. The second part, Γ, only depends on the exact form of the Lindblad jump operators $\mathcal{J}_\mu$ and captures the

dissipation. Non-Hermitian Hamiltonians, which encode only the dynamical part of the Lindblad time-evolution, have recently received a lot of interest in the context of non-Hermitian topology [20].

We continue by showing how to diagonalize the Liouvillian. There, it is necessary to preserve the bosonic structure given by the commutation relations. We encode them in

$$J_{ij} = [\boldsymbol{b}_i, \boldsymbol{b}_j] \quad \Rightarrow \quad J = \begin{pmatrix} 0 & I_{2m} \\ -I_{2m} & 0 \end{pmatrix}, \tag{2.25}$$

which is the standard symplectic form in Eq. (2.2). Thus, L and J are in the form of theorem 1 and we can find a symplectic transformation S that brings L in the normal form of Eq. (2.12).

2.2.2 Fixing the normal form

As it has been pointed out in remark 3, the generalized eigenvalues λ_i determine the stability of the system. Since they come in $\pm\lambda_i$ pairs, it is necessary to identify the correct eigenvalue $+\lambda_i$. One of the columns $\boldsymbol{s}_i$ and $\boldsymbol{s}_{i+n}$, $i \leq n$, of S is of the form $(\tilde{\boldsymbol{s}}_i, 0 \cdots 0)^T$, i.e. ending in n zeros, see [9]. If $\boldsymbol{s}_{i+n}$ ends in the zeros, we exchange $\boldsymbol{s}_i \mapsto -\boldsymbol{s}_{i+n}$ and $\boldsymbol{s}_{i+n} \mapsto \boldsymbol{s}_i$, while inverting the sign of $\lambda_i \mapsto -\lambda_i$, according to remark 3. Note that the normalization of the eigenvectors is given by $\boldsymbol{s}(-\lambda_i) J \boldsymbol{s}(\lambda_j) = \delta_{ij}$. In this way, we fix the signs of λ_i, while bringing the symplectic matrix in the block form

$$S = \begin{pmatrix} S_1 & S_2 \\ 0 & S_3 \end{pmatrix}. \tag{2.26}$$

The symplectic matrix has this form due to the fact that the noise given by N does not influence the spectrum. The condition $S^T J S = J$ implies that $S_3^T = S_1^{-1}$ and $S_2^T S_3 = S_3^T S_2$. In the following, we will always assume that the normal form is fixed in this way. Then, the generalized eigenvalue problem $L\boldsymbol{s}_i = \lambda_i J \boldsymbol{s}_i$ is equivalent to

$$H_{\text{eff}} \tilde{\boldsymbol{s}}_i = i\lambda_i Z \tilde{\boldsymbol{s}}_i \,, \tag{2.27}$$

which means that the eigenvalues λ_i of the Liouvillian are, up to multiplication by i, given by the eigenvalues of the non-Hermitian effective Hamiltonian H_{eff}. Previous methods solve Eq. (2.27) to diagonalize the effective Hamiltonian and then proceed by solving a Lyapunov equation to eliminate the noise N. This means that they obtain the diagonalized Liouvillian in a two-step process, see [9, 13]. Using the method that has been presented in this chapter, we combine the two steps into a single symplectic transformation. Below, we show how this brings an advantage when we turn to the task of counting, where the trace preservation is lost and the eigenvalues are not simply given by H_{eff}.

The transition to the normal form introduces new bosonic operators u_i and

v_i defined by

$$\boldsymbol{b} = S \begin{pmatrix} u_1 - \eta_1'/\lambda_1 \\ \vdots \\ u_n - \eta_n'/\lambda_n \\ v_1 \\ \vdots \\ v_n \end{pmatrix}, \tag{2.28}$$

which implies $\boldsymbol{b}_c = S_1(\boldsymbol{u} - \Lambda^{-1}\boldsymbol{\eta}') + S_2\boldsymbol{v}$ and $\boldsymbol{b}_q = S_3\boldsymbol{v}$. The linear terms $\boldsymbol{\eta}$ shift the vacuum as parameterized by the transformed vector $\boldsymbol{\eta}' = S_3^T\boldsymbol{\eta} = S_1^{-1}\boldsymbol{\eta}$.

As pointed out above, the bosonic structure is conserved due to the symplectic transformation. Therefore, they obey $[u_i, v_j] = \delta_{ij}$ and all other commutators vanish. Thus, u_i are annihilation and v_i creation operators, but they are not adjoints of each other. This follows from the fact that the Liouvillian is not Hermitian. Note that due to the special block form of S, the v_i are given by a linear combination of $\boldsymbol{a}_q$ and $\boldsymbol{a}_q^\dagger$. Because of this, the v_i also encode the trace preservation, see the discussion above.
Written with the new operators u_i and v_i, the Liouvillian assumes the form

$$\mathcal{L} = \sum_i \lambda_i v_i u_i, \tag{2.29}$$

where the additional constant $\frac{1}{2}\sum_i \lambda_i + L_0$ vanishes in accordance with the trace preservation. Note that $\sum_i \lambda_i = \mathrm{Tr}(-iZH_{\mathrm{eff}})$, see Eq. (2.27), which evaluates to $\mathrm{Tr}(W - V) = -2L_0$.

2.2.3 Fock space of the superoperator formalism

The ladder operators v_i, u_i introduce a Fock-like structure. The operator $v_i u_i$ is a number operator with eigenstates $|n_i\rangle$. Due to the ladder structure imposed by the commutation relation $[u_i, v_j] = \delta_{ij}$, we are able to obtain every eigenvalue and state starting from a single distinguished state. For the harmonic oscillator, this special role is taken by the vacuum state. Here, the trace preservation is the crucial ingredient, as it is the left eigenstate $\langle 0|$ of the Liouvillian with eigenvalue $\lambda = 0$. Starting from this state, we obtain the remaining states by application of u_i that acts as a creation operator to the left. The remaining states are then obtained by, $n_i \in \mathbb{N}_0$,

$$\langle n_1, n_2, \ldots| = \langle 0| \prod_{i=1}^{n} \frac{u_i^{n_i}}{\sqrt{n_i!}}, \tag{2.30}$$

which are left eigenstates of $v_i u_i$ to the eigenvalue n_i. Therefore, the spectrum of the Liouvillian $\mathcal{L}$ is given by

$$\lambda = \sum_{i=1}^{n} \lambda_i n_i \,. \tag{2.31}$$

Since the Liouvillian is not Hermitian, the right eigenvectors are not given by the adjoint of the left. The corresponding right eigenvectors are given by

$$|n_1, n_2, \ldots\rangle = \prod_{i=1}^{n} \frac{v_i^{n_i}}{\sqrt{n_i!}} |0\rangle \tag{2.32}$$

with the important right eigenvector $|0\rangle$ to the eigenvalue $\lambda = 0$. It corresponds to the stationary density matrix $\rho_s \equiv |0\rangle$ since $\mathcal{L}\rho_s = \dot{\rho_s} = 0$. The ladder operators act on the eigenstates $|n_1, n_2, \ldots\rangle = \bigotimes_i |n_i\rangle$ according to $u_i |n_i\rangle = \sqrt{n_i} |n_i - 1\rangle$ and $v_i |n_i\rangle = \sqrt{n_i + 1} |n_i + 1\rangle$ [2]. The action on the left eigenstates is given by $\langle n_i| u_i = \langle n_i + 1| \sqrt{n_i + 1}$ and $\langle n_i| v_i = \langle n_i - 1| \sqrt{n_i}$. These states form a complete bi-orthonormal set with $\langle n_1', n_2', \ldots | n_1, n_2, \ldots\rangle = \Pi_i \delta_{n_i', n_i}$ and the resolution of identity $I = \sum_{n_1, n_2, \ldots} |n_1, n_2, \ldots\rangle \langle n_1, n_2, \ldots|$. The completeness determines the time evolution operator of the Lindblad equation that equals

$$\exp(\mathcal{L}t) = \sum_{n_1, n_2, \ldots} e^{\lambda t} |n_1, n_2, \ldots\rangle \langle n_1, n_2, \ldots| , \tag{2.33}$$

with $\lambda = \sum_i \lambda_i n_i$. This means that states with large λ (large n_i or λ_i) decay faster than others. This allows to adiabatically eliminate the fast modes, which will be demonstrated in Ch. 4 and Ch. 5.

Jordan normal form

Generally, it might happen that the matrix $J^{-1}L$ is not diagonalizable, meaning that it can only be brought into its Jordan normal-form. For the following, we will discuss the simplest case for a system containing a single boson where the eigenvalues and eigenvectors coalesce. In this case, the Liouvillian equals $\mathcal{L} = \mu(v_1 u_1 + v_2 u_2) + \nu v_2 u_1$, where the first part is diagonal and $v_2 u_1$ is nilpotent. While we discuss the case of a single boson and therefore also a single Jordan block, the following procedure can be generalized to a larger number of bosons with larger Jordan blocks.

While the algebraic eigenvalues of $\mathcal{L}$ stays the same, the geometrical spectrum that determines the dynamics of the system changes. If $\mathcal{L}$ would be diagonalizable with degenerate eigenvalues, there would be a degeneracy of $n+1$ for each eigenvalue $\lambda = \mu(n_1 + n_2)$ with $n_1 + n_2 = n$. Because a complete decomposition of $\mathcal{L}$ by eigenstates is not possible anymore, additional generalized eigenstates are needed. Acting with the Liouvillian on the Fock-states, we obtain

$$\mathcal{L} |n_1, n_2\rangle = \mu(n_1 + n_2) |n_1, n_2\rangle + \nu \sqrt{n_1(n_2 + 1)} |n_1 - 1, n_2 + 1\rangle . \tag{2.34}$$

We see that, for fixed $n = n_1 + n_2$, only the state $|0, n\rangle$ with $n_1 = 0$ is an eigenstate of the Liouvillian. The n remaining states $|n_1, n - n_1\rangle$ with $n_1 =$

[2] It would be also possible to choose a different 'normalization' of the operators, e.g. $u_i |n_i\rangle = |n_i - 1\rangle$ and $v_i |n_i\rangle = (n_i + 1) |n_i + 1\rangle$ since they are not adjoints of each other.

$1, \ldots, n$ are *generalized* eigenstates. The time evolution operator reads

$$e^{\mathcal{L}t} = \sum_{\substack{n_1,n_2\geq 0 \\ 0\leq m\leq n_1}} \sqrt{\binom{n_1}{m}\binom{n_2+m}{m}}\,(\nu t)^m e^{\mu(n_1+n_2)t}\,|n_1-m, n_2+m\rangle\langle n_1, n_2|\ , \tag{2.35}$$

where m runs over the set of generalized eigenstates to a fixed n. The time evolution is not a simple sum of exponential terms anymore. This is due to the fact that the eigenstates do not form a complete basis anymore and generalized eigenstates are needed. They change the dynamics because of the nilpotent operator $v_2 u_1$.

2.3 Counting statistics

When solving the Lindblad equation, not only the stationary state and the spectrum that determine the time evolution are of interest. Often, one is concerened with the statistics of observables $\mathcal{O}$ such as the photon current. The statistics are accessible by determining the corresponding cumulant generating function $\mathcal{G}(s)$. In this section, we show to obtain the generating function using the symplectic transformation of theorem 1.

We are able to access the statistics by including a source term in the Liouvillian superoperator [5, 21]

$$\mathcal{L}(s) = \mathcal{L} + s\mathcal{O}. \tag{2.36}$$

with $s \in \mathbb{C}$. The (super-)operator $\mathcal{O}$ represents the process that we want to observe, and should be again of quadratic order for solvability. A common example is the emission of single photons, expressed by the process $a\rho a^\dagger$. The corresponding superoperator that describes this is then given by $\mathcal{I} = a_+ a_-^\dagger$. By inclusion of the source term, the diagonalized Liouvillian $\mathcal{L}(s)$ reads

$$\mathcal{L}(s) = \sum_i \lambda_i(s) v_i(s) u_i(s) + \frac{1}{2}\sum_i \lambda_i(s) + L_0. \tag{2.37}$$

Note that by including the source term, the trace preservation of the Lindblad equation is lost. This means that the upper left block, that encodes this property, gets replaced by a symmetric matrix $C(s)$ with $C(0) = 0$. Here, we see another advantage of the symplectic transformation. As mentioned above, previous methods are able to diagonalize the Liouvillian by eliminating the noise N due to the vanishing upper-left block in Eq. 2.19. The symplectic transformation does not run into this problem and can still be used to diagonalize $\mathcal{L}(s)$. Here, the eigenvalues $\lambda(s)$ and ladder operators $v(s), u(s)$ are choosen as a function of s that result in the normal eigenvalues λ and ladder operators v, u as $s \to 0$. This is important since we are not able to use the trace preservation anymore to distinguish the sign of the symplectic eigenvalues $\pm\lambda(s)$.

The factorial cumulant generating function $\mathcal{G}(s)$ for a measurement time τ is defined by

$$e^{\mathcal{G}(s)\tau} = \langle 0| \, e^{\mathcal{L}(s)\tau} \, |0\rangle = \mathrm{Tr}\big(e^{\mathcal{L}(s)\tau}\rho_s\big) \, . \tag{2.38}$$

The derivatives with respect to s evaluated at $s = 0$ produce the factorial cumulants [21–23]

$$\langle\!\langle \mathcal{O}^k \rangle\!\rangle_F = \langle\!\langle \mathcal{O}(\mathcal{O}-1)\cdots(\mathcal{O}-k+1) \rangle\!\rangle = \frac{d^k}{ds^k}\mathcal{G}(s)\bigg|_{s=0} \, . \tag{2.39}$$

Note that the conventional cumulants can be obtained by replacing $s \mapsto \exp(i\chi) - 1$ and taking the derivative with respect to $i\chi$ [23]. In the limit of long measurement time with $-\mathrm{Re}(\lambda_i)\tau \gg 1$, only the term with $n_i = 0$ (the stationary state) contributes in (2.33). The factorial cumulant generating function is then given by

$$\mathcal{G}(s) = \langle 0| \, \mathcal{L}(s) \, |0\rangle = \frac{1}{2}\sum_i \lambda_i(s) + L_0 = \frac{1}{2}\sum_i \big[\lambda_i(s) - \lambda_i(0)\big] \, . \tag{2.40}$$

To obtain the generating function $\mathcal{G}(s)$ analytically with the presented method, we require a quadratic Liouvillian and observable. If this is not the case anymore, e.g. when the Hamiltonian contains a nonlinearity as it will be the case in Ch. 4 and 5, we are not able to use the diagonalization to obtain the generating function. But, we are able to obtain the (factorial) cumulants by perturbation theory. Because we evaluate the generating function at $s = 0$, we can see s as a small parameter and therefore the source term as a small perturbation. Expanding the generating function at $s = 0$ yields

$$\mathcal{G}(s) = \sum_{k=1}^{\infty} \frac{1}{k!} \langle\!\langle \mathcal{O}^k \rangle\!\rangle_F \, s^k. \tag{2.41}$$

This means that we are able to access the coefficient of the expansion $\langle\!\langle \mathcal{O}^k \rangle\!\rangle_F / k!$ by using k-th order (non-Hermitian) perturbation theory, and we obtain the factorial cumulants by multiplication of $k!$.

2.4 Examples

In the last section of this chapter, we demonstrate how to use the method of 'third quantization' for two examples. First, we diagonalize the Liouvillian of the harmonic oscillator that is subject to single photon loss, and derive the generating function of the photon current. Afterwards, we give an example for a non-diagonalizable system where Jordan blocks appear.

2.4.1 Symplectic diagonalization and counting

The Lindblad master equation that describes the damped harmonic oscillator, with frequency ω and dissipation rate γ, can be constructed by the Hamiltonian

$H = \omega a^\dagger a$ and the Lindblad jump operators

$$\mathcal{J}_1 = \sqrt{\gamma(\bar{n}+1)}\, a \quad \text{and} \quad \mathcal{J}_2 = \sqrt{\gamma\bar{n}}\, a^\dagger. \tag{2.42}$$

The first one relates to sponteanous and induced emission of a single photon, while the latter corresponds to the absorption of a photon from the environment with the Bose-Einstein occupation $\bar{n}$. The effective Hamiltonian and noise matrix read

$$H_{\text{eff}} = \begin{pmatrix} \omega + \frac{i}{2}\gamma & 0 \\ 0 & \omega - \frac{i}{2}\gamma \end{pmatrix}, \quad N = \frac{1}{2}\begin{pmatrix} 0 & \gamma(2\bar{n}+1) \\ \gamma(2\bar{n}+1) & 0 \end{pmatrix}. \tag{2.43}$$

The symplectic transition matrix that diagonalizes the Liouvillian is given by

$$S = \begin{pmatrix} 1 & 0 & 0 & \bar{n}+\frac{1}{2} \\ 0 & 1 & \bar{n}+\frac{1}{2} & 0 \\ 0 & 0 & 1 & 0 \\ 0 & 0 & 0 & 1 \end{pmatrix}. \tag{2.44}$$

We clearly see that the transformation matrix has the block form given in Eq. (2.26). The diagonalized Liouvillian reads

$$\mathcal{L} = \left(-i\omega - \frac{\gamma}{2}\right) v_1 u_1 + \left(i\omega - \frac{\gamma}{2}\right) v_2 u_2. \tag{2.45}$$

Note that the spectrum is given by $\lambda = \mu n_1 + \mu^* n_s$ with $\mu = -i\omega - \gamma/2$. Therefore, the eigenvalues λ are either real there are complex conjugate pairs. This property is addressed in the next chapter.

Next, we show how to obtain the generating function for the outgoing photon current $\mathcal{I} = \gamma a_+ a_-^\dagger$. We add a source term to the Liouvillian which now reads

$$\mathcal{L}(s) = \mathcal{L} + s\mathcal{I}. \tag{2.46}$$

The eigenvalues of $\mathcal{L}(s)$ are given by $\pm\frac{1}{2}(\gamma\sqrt{1-4\bar{n}s}+2i\omega)$ and $\pm\frac{1}{2}(\gamma\sqrt{1-4\bar{n}s}-2i\omega)$. We can compare this to Eq. (2.45) for $s=0$ and identify the eigenvalues with the negative sign as the correct eigenvalues. We obtain the generating function [21]

$$\mathcal{G}(s) = \frac{1}{2}\sum_i \big[\lambda_i(s) - \lambda_i(0)\big] = \frac{\gamma}{2}\big(1 - \sqrt{1-4\bar{n}s}\big). \tag{2.47}$$

2.4.2 Jordan decomposition

Here, we provide an example for a 1-boson system where Jordan blocks appear. The Hamiltonian is given by

$$\mathcal{H} = \frac{\Delta}{2} a^\dagger a + \frac{i\epsilon}{4}\left(a^{\dagger 2} - a^2\right). \tag{2.48}$$

It has a physical realization as the degenerate parametric oscillator in the rotating frame with detuning Δ and driving strength $\epsilon > 0$, which will also be

discussed in Ch. 4. The coupling to the environment is again modeled by single photon loss given by the jump operators in Eq. (2.42). The effective Hamiltonian and noise matrix read

$$H_{\text{eff}} = \frac{1}{2}\begin{pmatrix} \Delta - i\gamma & i\epsilon \\ -i\epsilon & \Delta + i\gamma \end{pmatrix}, \quad N = \frac{1}{2}\begin{pmatrix} 0 & \gamma(2\bar{n}+1) \\ \gamma(2\bar{n}+1) & 0 \end{pmatrix}. \tag{2.49}$$

For $\epsilon = \Delta$, the Liouvillian matrix L is not diagonalizable and therefore the Jordan decomposition is needed [12]. The symplectic transition matrix

$$S = \begin{pmatrix} 1 & -i & \frac{(\epsilon+i\gamma)(2\bar{n}+1)}{2\gamma} & \frac{(\epsilon^2+\gamma^2)(2\bar{n}+1)}{2\gamma^2} \\ 0 & 1 & \frac{(i\epsilon+\gamma)(2\bar{n}+1)}{2\gamma} & \frac{\epsilon(i\epsilon+\gamma)(2\bar{n}+1)}{2\gamma^2} \\ 0 & 0 & 1 & 0 \\ 0 & 0 & i & 1 \end{pmatrix} \tag{2.50}$$

brings the Liouvillian onto the form $\mathcal{L} = -\frac{\gamma}{2}(v_1u_1 + v_2u_2) + \frac{\epsilon}{2}v_2u_1$. Again, the transition matrix S fulfills the condition of trace preservation since the lower-left block vanishes. The time evolution is given by Eq. (2.35) with $\mu = -\frac{\gamma}{2}$ and $\nu = \frac{\epsilon}{2}$.

Chapter 3

Symmetries

Symmetries are a powerful tool to get deeper insight into a system. For Hamiltonian systems, a symmetry demands that the Hamiltonian H commutes with a unitary symmetry operator Ω. First attempts to generalize the ideas of symmetries to the Lindblad equation have been studied in Ref. [24, 25]. In the following, we approach this problem by using the superoperator formalism and the structure of the Lindblad equation that has been introduced above.

3.1 Hermiticity of the density matrix

Every density matrix has three fundamental properties. It is Hermitian ($\rho = \rho^\dagger$), positive semi-definite ($\rho \geq 0$), and normalized ($\mathrm{Tr}(\rho) = 1$). These properties must be preserved under any transformation. It is known that the Lindblad master equation is CPTP, completely positive and trace preserving. Only the hermiticity and the restrictions that it puts onto the Liouvillian are left out in discussions. Here, we want to address this property.

The most general form of a density matrix expressed in an orthonormal basis $|n\rangle = |n_1, n_2, ...\rangle$ is represented by

$$\rho = \sum_{m,n} \rho_{mn} |m\rangle\langle n| \tag{3.1}$$

with $\rho_{mn} = \rho^*_{nm}$ due to hermiticity. The superoperator formalism introduces a vectorization of the density matrix. The vectorized density matrix then reads

$$|\rho\rangle = \sum_{m,n} \rho_{mn} \, |m, n\rangle \tag{3.2}$$

where $|m, n\rangle = |m\rangle \otimes |n\rangle$. Since the meaning of hermiticity in this form is not clear, we want to define an adjoint operator $\mathcal{A}$. We motivate it by the definition of the conventional adjoints of matrices, transposing the matrix and taking the complex conjugate. It therefore acts as $\mathcal{A}\, z \, |m, n\rangle = z^* \, |n, m\rangle$. Then, $\mathcal{A}$ is expressed as an anti-unitary operator in the product basis as

$$\mathcal{A} = \sum_{m,n} |n, m\rangle \, \langle m, n| \, K \tag{3.3}$$

where K is complex conjugation and $\mathcal{A}^2 = I$. It leaves the vectorized density matrix invariant with

$$\mathcal{A}\,|\rho\rangle = \sum_{m,m',n,n'} \rho^*_{mn}\,|n',m'\rangle \underbrace{\langle m'|m\rangle}_{\delta_{m,m'}} \underbrace{\langle n'|n\rangle}_{\delta_{n,n'}} = \sum_{m,n} \rho_{nm}\,|n,m\rangle = |\rho\rangle\,. \tag{3.4}$$

Since the hermiticity cannot be broken under time evolution, it follows that $[\mathcal{A}, \mathcal{L}] = 0$.

To see the restriction that the hermiticity puts upon the Liouvillian, we also investigate the action of $\mathcal{A}$ on the superoperators. This means that

$$\mathcal{A}\,|m,n\rangle = \frac{(\mathcal{A}a_+^\dagger\mathcal{A})^m}{\sqrt{m!}} \frac{(\mathcal{A}a_-\mathcal{A})^n}{\sqrt{n!}} \mathcal{A}\,|0\rangle \overset{!}{=} \frac{(a_-)^m}{\sqrt{m!}} \frac{(a_+^\dagger)^n}{\sqrt{n!}}\,|0\rangle = |n,m\rangle\,, \tag{3.5}$$

since the stationary state $|0\rangle = |0,0,..,0\rangle$ is Hermitian with $\mathcal{A}\,|0\rangle = |0\rangle$. Thus, $\mathcal{A}a_+^\dagger\mathcal{A} = a_-$ and $\mathcal{A}a_-\mathcal{A} = a_+^\dagger$. This means that $\mathcal{A}a_c\mathcal{A} = a_c^\dagger$ and $\mathcal{A}a_q\mathcal{A} = -a_q^\dagger$. In a first quantized version in the basis $\boldsymbol{b} = (\boldsymbol{a}_c, \boldsymbol{a}_c^\dagger, \boldsymbol{a}_q^\dagger, -\boldsymbol{a}_q)^T$ this operation equals

$$A = \begin{pmatrix} X & 0 \\ 0 & X \end{pmatrix} K \qquad \text{where} \qquad X = \begin{pmatrix} 0 & I_m \\ I_m & 0 \end{pmatrix}. \tag{3.6}$$

The hermiticity constraint requires that $ALA = L$ and thus $XH^*_{\text{eff}}X = H_{\text{eff}}$ and $XN^*X = N$. It also preserves the bosonic structure encoded in the symplectic form, $AJA = J$. Additionally, the hermiticity puts a restriction on the observable $\mathcal{O}$ when a source term is involved in the Liouvillian, see Eq. (2.36). It requires that $[\mathcal{A}, \mathcal{O}] = 0$. For example, the photon current $\mathcal{I} = \gamma a_+ a_-^\dagger$ fulfills this by

$$\mathcal{A}\mathcal{I}\mathcal{A} = \gamma(\mathcal{A}a_+\mathcal{A})(\mathcal{A}a_-^\dagger\mathcal{A}) = \gamma a_-^\dagger a_+ = \gamma a_+ a_-^\dagger = \mathcal{I}. \tag{3.7}$$

The fact that the density matrix is hermitian also explains the fact that the Liouvillian has either real eigenvalues or there are complex conjugate pairs. Given a generalized eigenvector $\boldsymbol{s}_i$ to the eigenvalue λ_i of the Liouvillian $L\boldsymbol{s}_i = \lambda_i J\boldsymbol{s}_i$, the vector $A\boldsymbol{s}_i = \boldsymbol{s}_i'$ is an eigenvector to the eigenvalue λ_i^*. This can be shown by the straightforward calculation

$$L\boldsymbol{s}_i' = LA\boldsymbol{s}_i = AL\boldsymbol{s}_i = \lambda_i^* AJA\boldsymbol{s}_i' = \lambda_i^* J\boldsymbol{s}_i'\,. \tag{3.8}$$

Due to this, the eigenvalues λ_i are either real or come in complex conjugate pairs, see Fig 3.1 where we show the key characteristics of the spectrum. For real eigenvalues, the eigenvectors $\boldsymbol{s}_i$ can be choosen in such a way that they fulfill $A\boldsymbol{s}_i = \boldsymbol{s}_i$.

3.2 Symmetries of the Lindblad master equation

For unitary dynamics, a Hamiltonian $\mathcal{H} = \frac{1}{2}\boldsymbol{b}^\dagger H\boldsymbol{b}$ in the basis $\boldsymbol{b} = (\boldsymbol{a}, \boldsymbol{a}^\dagger)^T$ may contain a symmetry. This is implemented by a unitary matrix Ω [1] that

[1] The case of an anti-unitary Ω is discussed below.

transforms $\boldsymbol{b} \mapsto \Omega\boldsymbol{b}$ and fulfills $\Omega^\dagger H\Omega = H$. Moreover, it has to fulfill $\Omega^\dagger\, iZ\,\Omega = iZ$ to preserve the bosonic structure and $X\Omega^* X = \Omega$ to keep $a_i^\dagger$ the adjoint of a_i. As a symmetry of the effective Hamiltonian $H_{\text{eff}} = H + i\Gamma$, we extend the symmetry of the Hamiltonian to $\Omega^\dagger H_{\text{eff}}\Omega = H_{\text{eff}}$. We then elevate the symmetry to the full Liouvillian by $\tilde{\Omega}^T L\tilde{\Omega} = L$ with

$$\tilde{\Omega} = \begin{pmatrix} \Omega & 0 \\ 0 & \Omega^* \end{pmatrix}. \tag{3.9}$$

The full symmetry $\tilde{\Omega}$ is unitary and symplectic, with $\tilde{\Omega}^T J\tilde{\Omega} = J$. It also commutes with the hermiticity $[A, \tilde{\Omega}] = 0$. This means that if Ω is anti-unitary, we are able to choose ΩXK as a unitary symmetry.

The symmetry $\tilde{\Omega}^T L\tilde{\Omega} = L$ requires that

$$\Omega^\dagger H_{\text{eff}}\Omega = H_{\text{eff}} \qquad \text{and} \qquad \Omega N\Omega^T = N\,. \tag{3.10}$$

The requirements $\Omega^\dagger iZ\Omega = iZ$ (preservation of bosonic structure) and $X\Omega^* X = \Omega$ (hermiticity) demands that Ω is of the form

$$\Omega = \begin{pmatrix} P & 0 \\ 0 & P^* \end{pmatrix} \tag{3.11}$$

with P being a unitary matrix. Therefore, a symmetry requires that

$$\begin{aligned} &P^\dagger hP = h, \qquad && P^T\Delta P = \Delta, \qquad && P\boldsymbol{z} = \boldsymbol{z}, \\ &P^T UP = U, \qquad && P^\dagger WP = W, \qquad && P^T VP^* = V \end{aligned} \tag{3.12}$$

on the parts of H_{eff}, N, and the linear contributions $\boldsymbol{z}$. We discuss an example of a unitary symmetry in Sec. 3.4.

3.3 $\mathcal{PT}$-'symmetry'

$\mathcal{PT}$-'symmetry' has been proposed as an alternative to the conventional unitary quantum mechanics [26]. There, the requirement of an Hermitian Hamiltonian $\mathcal{H}^\dagger = \mathcal{H}$ is lifted and replaced by the weaker constraint of a $\mathcal{PT}$-'symmetric' Hamiltonian, $[\mathcal{PT}, \mathcal{H}] = 0$. The Hamiltonian still has real eigenenergies E in the $\mathcal{PT}$-'symmetric' phase. But if the $\mathcal{PT}$-'symmetry' is broken, the eigenenergies come in complex conjugate pairs E, E^*. Then, the $\lambda = -iE$ that determine the time evolution, see Eq. (2.27), come in pairs of λ and $-\lambda^*$.

In open quantum systems, $\mathcal{PT}$-'symmetry' is realized when the absorption and the emission counteract each other. An unbroken 'symmetry' leads to purely imaginary λ. More generally, it demands that for each λ, $-\lambda^*$ is also part of the spectrum, see above and Fig. 3.1. In our description, a $\mathcal{PT}$-'symmetry' is realized for an anti-unitary Ω with $\Omega^\dagger H_{\text{eff}}\Omega = H_{\text{eff}}$ and $\Omega^\dagger iZ\Omega = -iZ$. The latter condition implements an exchange of the roles of the creation and annihilation operators. This indicates the balance of gain and loss, see below. The

anti-unitarity maps $\lambda \mapsto \lambda^*$ while the reversal of iZ introduces a minus sign and we therefore obtain pairs of λ and $-\lambda^*$. The hermiticity requirement still holds with $X\Omega^* X = \Omega$.

Similar to the previous section, we can elevate this to a 'symmetry' $\tilde{\Omega}^T L \tilde{\Omega} = L$ of the full Liouvillian with

$$\tilde{\Omega} = \begin{pmatrix} \Omega & 0 \\ 0 & -\Omega \end{pmatrix}, \tag{3.13}$$

while $\tilde{\Omega}^T J \tilde{\Omega} = -J$ which encodes the interchange of creation and annihilation operators. The hermitcity requires $[A, \tilde{\Omega}] = 0$. Then, the blocks of Ω are fixed as

$$\Omega = \begin{pmatrix} P & 0 \\ 0 & P \end{pmatrix} K \tag{3.14}$$

with a real orthogonal and symmetric matrix $P = P^T$. This connects to the more conventional definition of $\mathcal{PT}$-'symmetry', where the time reversal is implemented by K and the parity operator by a unitary P. The action on the individual parts of the blocks in H_{eff} and N are given by

$$\begin{aligned} &Ph^*P = h, \qquad &&P\Delta^*P = \Delta, \qquad &&P\boldsymbol{z} = -\boldsymbol{z}^*, \\ &PUP = U^\dagger, \qquad &&PWP = V\,. \end{aligned} \tag{3.15}$$

Therefore, systems with $\mathcal{PT}$-'symmetry' can be identified by two properties. First, the Hamiltonian of the system is $\mathcal{PT}$-symmetric by itself. Second, the dissipative, non-unitary part of the Lindblad equation is invariant for an interchange of the gain and loss processes. Our definition of $\mathcal{PT}$-'symmetry' in Eq. (3.13) is a generalization of the one proposed in [27,28]. In the case that the $\mathcal{PT}$-'symmetry' is unbroken with $\mathrm{Re}(\lambda_i) = 0$ [2], the eigenstates can be choosen such that $\tilde{\Omega}\boldsymbol{s}_i = \boldsymbol{s}_i$. In the case of broken 'symmetry', acting with $\tilde{\Omega}$ maps an eigenstate with eigenvalue λ_i to its partner with eigenvalue $-\lambda_i^*$; the proof follows equivalent to the proof presented in Eq. (3.8). In the next section, we provide examples for a unitary symmetry and the $\mathcal{PT}$-'symmetry'.

3.4 Examples

3.4.1 Unitary symmetries

We start with the unitary symmetries of the degenerate parametric oscillator, presented in Sec. 2.4.2. It contains two symmetries. First, the model has a $U(1)$-symmetry at $\epsilon = 0$ and is implemented by $P = e^{i\phi}$ where $\phi \in \mathbb{R}$. This corresponds to the unitary matrix

$$\Omega = \begin{pmatrix} e^{i\phi} & 0 \\ 0 & e^{-i\phi} \end{pmatrix}. \tag{3.16}$$

For parametric driving with $\epsilon > 0$, the $U(1)$-symmetry is broken to a $\mathbb{Z}_2$-symmetry. Then, $\phi = 0, \pi$ and the remaining symmetry operations $\Omega = \pm I_2$.

[2] The eigenvalues $\lambda = -iE$ have $\mathrm{Re}(\lambda_i) = 0$ since the eigenenergies E are real in the unbroken phase.

The latter symmetry is always present for quadratic system, meaning when $\boldsymbol{z} = 0$ in Eq. (2.20).

3.4.2 $\mathcal{PT}$-'symmetry' in coupled harmonic oscillators

Here, we discuss an example for a Liouvillian $\mathcal{PT}$-'symmetric' system containing two bosonic modes. The Hamiltonian is given by, see [27, 29],

$$\mathcal{H} = \frac{g}{2}(ab^\dagger + a^\dagger b). \tag{3.17}$$

It describes two coupled oscillators exchanging excitations with a coupling strength g. The dissipation is modelled by

$$\mathcal{J}_1 = \sqrt{\gamma_l}\, a, \qquad \mathcal{J}_2 = \sqrt{\gamma_g}\, b^\dagger\,, \tag{3.18}$$

where γ_l describes the loss rate of mode a and γ_g the gain rate of mode b. The relevant matrices to identify the $\mathcal{PT}$-'symmetry' are given by

$$H_{\text{eff}} = \frac{1}{2}\begin{pmatrix} h_{\text{eff}} & 0 \\ 0 & h_{\text{eff}}^* \end{pmatrix}, \qquad N = \frac{1}{2}\begin{pmatrix} 0 & n \\ n & 0 \end{pmatrix} \tag{3.19}$$

with

$$h_{\text{eff}} = \begin{pmatrix} -i\gamma_l & g \\ g & i\gamma_g \end{pmatrix}, \qquad n = \begin{pmatrix} \gamma_l & 0 \\ 0 & \gamma_g \end{pmatrix}. \tag{3.20}$$

At the point $\gamma_l = \gamma_g = \gamma$ where the gain matches the loss, the system shows a $\mathcal{PT}$-'symmetry' with $P = X$. This corresponds to the anti-unitary symmetry matrix

$$\Omega = \begin{pmatrix} X & 0 \\ 0 & X \end{pmatrix} K\,. \tag{3.21}$$

At the $\mathcal{PT}$-'symmetric' point, the spectrum is given by $\lambda = \pm i\sqrt{g^2 - \gamma^2}/2$ with double degenerate eigenvalues. For $\gamma < |g|$, the $\mathcal{PT}$-'symmetry' is unbroken, and the eigenvalues are purely imaginary. Still, due to the appearance of Jordan blocks, the time-evolution grows polynomial in time, see Eq.(2.35) and Ref. [24] For larger dissipation $\gamma > |g|$, the $\mathcal{PT}$-'symmetry' is broken and the dynamics diverge exponentially.

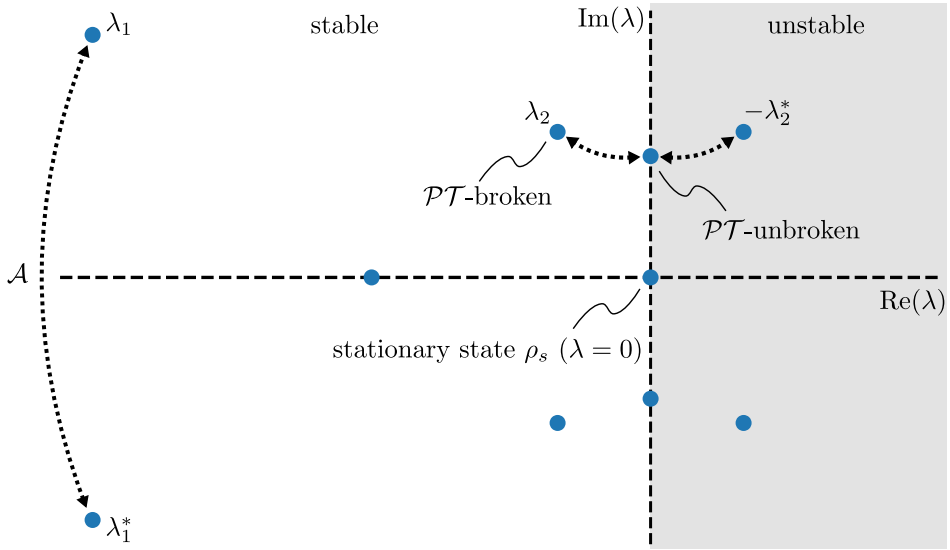

Figure 3.1: Sketch of the spectrum of a Liouvillian showing the key characteristics. The eigenvector $|0\rangle$ to the eigenvalue $\lambda = 0$ corresponds to the stationary state ρ_s. States with eigenvalue $\mathrm{Re}(\lambda) < 0$ decay exponentially and relax to the stationary state. Eigenvalues with $\mathrm{Re}(\lambda) > 0$ (grey shaded region) indicate that the system is unstable and the time-evolution $\exp(\mathcal{L}t)$ diverges exponentially. The mirroring of the spectrum along the real axis is due to the hermitcity of the density-matrix $\rho(t)$ encoded in the adjoint operator $\mathcal{A}$ with $[\mathcal{A}, \mathcal{L}] = 0$. Similarly for a $\mathcal{PT}$-symmetry, the eigenvalues come in pairs mirrored along the imaginary axis. If all the eigenvalues are on the imaginary axis (corresponding to unitary dynamics), the $\mathcal{PT}$-symmetry is called unbroken. In the opposite case with a broken $\mathcal{PT}$-symmetry, the system is unstable as one of the pair of eigenvalues has a positive real part.

Chapter 4

Degenerate parametric oscillator

The goal of this chapter is to introduce the reader to parametric resonance, specifically to the degenerate parametric oscillator, where a single oscillator is driven parametrically at twice its natural frequency. When the driving strength exceeds the damping, also called instability threshold, self-sustained coherent oscillations are possible. For the quantum mechanical equivalent, quantum fluctuations enable the emission of photons already below this threshold. The resulting radiation statistics have been analyzed in Ref. [6]. This chapter provides a review and also additional results of Ref. [6] to present the main ideas and methods that have been used to derive an effective model of this system. In the next chapter, we look into the non-degenerate parametric oscillator, where two oscillators with different frequencies Ω_a and Ω_b are parametrically driven at the sum of their frequencies. By discussing the degenerate case first, we are able to compare to the non-degenerate case and point out differences as well as similarities.

4.1 Short introduction to parametric resonance

A degenerate parametric oscillator with amplitude x is described by the differential equation

$$\ddot{x} + \gamma\dot{x} + x\left[\Omega^2 + 2\Omega\epsilon\sin(\Omega_d t)\right] = 0. \tag{4.1}$$

The first three terms correspond to a damped harmonic oscillator with the natural frequency Ω and damping rate γ. The last term encodes the parametric drive. We see that it corresponds to a modulation of Ω with a driving strength ϵ and a driving frequency Ω_d. When the driving frequency equals twice the natural frequency, $\Omega_d = 2\Omega$, we achieve parametric resonance. This shows itself in the form of coherent oscillations with a relative phase of 0 and π with respect to the drive when the driving strength exceeds the damping. This point is also called instability threshold, which is discussed in the following.

To solve Eq. (4.1), we choose the Ansatz $x(t) = x_1(t)\cos(\Omega t) + x_2(t)\sin(\Omega t)$. Then, the product $x(t)\sin(2\Omega t)$ produces two driving signals by employing

trigonometric properties. There are resonant driving terms with frequency Ω and non-resonant terms that oscillate with 3Ω. We perform a rotating wave approximation, where the fast oscillations that are non-resonant are neglected. We also assume that the quadratures x_1 and x_2 vary slowly and $\gamma, \epsilon \ll \Omega$. This leads to

$$\dot{x_1} = -\frac{\gamma - \epsilon}{2} x_1 \qquad \text{and} \qquad \dot{x_2} = -\frac{\gamma + \epsilon}{2} x_2. \tag{4.2}$$

In this form, we can identify the threshold. For $\epsilon > \gamma$, the first quadrature x_1 is exponentially amplified, while the second quadrature x_2 is suppressed. This is why the degenerate parametric oscillator is able to realize phase-sensitive amplification. This property can also be identified, when we write Eq. (4.2) in terms of the complex amplitude $A = (x_1 + ix_2)/\sqrt{2}$. The corresponding differential equation reads $\dot{A} = -(\gamma/2)A + (\epsilon/2)A^*$. While the damping is always present, we see that the drive couples to the complex conjugate. Therefore, the real part of A can be amplified while the imaginary part is suppressed. At threshold ($\epsilon \approx \gamma$), the first quadrature accurately describes the relevant slow dynamics of the system because the decay rate $(\gamma - \epsilon)/2$ is small. In comparison, x_2 decays exponentially fast with rate γ. Because of this property, we are able to reduce the dynamics of the system to the first quadrature x_1 when we are close to the threshold. In the linearized theory of the harmonic oscillator, this threshold relates to an instability, since the first quadrature diverges exponentially. At this point, it is necessary to take anharmonicities of the oscillator into account that cures the divergence and stabilizes the system again. The oscillator is then described by the Langevin equation

$$\dot{x} = -\frac{\gamma}{2}x + f(x) + \sqrt{\gamma\left(\bar{n} + \frac{1}{2}\right)}\,\xi, \tag{4.3}$$

where we have included the white noise $\langle \xi(t)\xi(t')\rangle = \delta(t - t')$ with the Bose-Einstein-occupation $\bar{n} = (e^{\hbar\Omega/k_B T} - 1)^{-1}$. The drift that characterizes the oscillator equals $f(x) \approx \frac{1}{2}\epsilon x - \gamma\alpha x^{m+1}$, where $\alpha \ll 1$ and the even valued, natural number m describe the anharmonicitiy of the oscillator. While $m = 2$ is the generic case that fulfills the $\mathbb{Z}_2$-symmetry, it is worth noting that the Duffing oscillator realizes $m = 4$. Below threshold, self-sustained oscillations are not possible and x approaches the stationary state x_s at the origin, $x_s = 0$. Above threshold, two stable solutions emerge with $x_s \propto \pm[(\epsilon - \gamma)/\alpha]^{1/m} \gg 1$ where the sign relates to the different phase-shifts of 0 and π.

4.2 Effective Liouvillian of slow dynamics

As shown above, classical self-sustained oscillations are not possible below the threshold. In the quantum regime, quantum fluctuations enable emission of photons already below threshold. The process is called parametric down-conversion and describes the phenomenon when a photon with frequency 2Ω turns into a pair of photons with frequency Ω. The model has been previously studied theoretically in Ref. [30] below the classical instability. In this regime, the nonlinearity is not important yet and quantum fluctuations play the largest

role. When we approach the threshold, the outgoing photon current diverges as it is for the classical case. Close to this instability, a nonlinearity has to be included. Far above threshold, the system reaches the classical regime, where it is described by a coherent state and the radiation statistics follow a Poissonian distribution. In this regime, the nonlinearity plays the relevant role to describe the dynamics of the system. In the close vicinity of the threshold however, both quantum fluctuations and the nonlinearity have to be included to obtain an accurate description of the dynamics. To demonstrate how to obtain a model that describes this critical regime, we start by solving the according Lindblad equation, using the method described in Ch 2.

In the rotating frame and without dissipation, the parametric oscillator can be described by the Hamiltonian

$$H = \frac{i\epsilon}{4}\big(a^{\dagger 2} - a^2\big), \tag{4.4}$$

see e.g. [31]. The dissipation is modeled by single photon loss described by the Lindblad jump operators

$$\mathcal{J}_1 = \sqrt{\gamma(\bar{n}+1)}\, a \quad \text{and} \quad \mathcal{J}_2 = \sqrt{\gamma\bar{n}}\, a^\dagger \tag{4.5}$$

that relate to induced and spontaneous emission by $\mathcal{J}_1$ and absorption by $\mathcal{J}_2$. The effective Hamiltonian and noise matrix of the corresponding Lindblad equation read

$$H_{\text{eff}} = \frac{1}{2}\begin{pmatrix} -i\gamma & i\epsilon \\ -i\epsilon & i\gamma \end{pmatrix} \quad \text{and} \quad N = \frac{1}{2}\begin{pmatrix} 0 & \gamma(2\bar{n}+1) \\ \gamma(2\bar{n}+1) & 0 \end{pmatrix}. \tag{4.6}$$

The diagonalized Liouvillian reads

$$\mathcal{L}_{\text{quad}} = -\frac{1}{2}(\gamma-\epsilon)v_s u_s - \frac{1}{2}(\gamma+\epsilon)v_f u_f. \tag{4.7}$$

The subscripts of the transformed ladder operators indicate the slow and fast decaying modes. We find that the decay rates in Eq. (4.7) matches the classical expectation. The creation and annihilation operators given by

$$\begin{aligned} u_s &= x_c + i\frac{\gamma(2\bar{n}+1)}{2(\gamma-\epsilon)}y_q, \quad v_s = -iy_q \\ u_f &= y_c - i\frac{\gamma(2\bar{n}+1)}{2(\gamma+\epsilon)}x_q, \quad v_f = ix_q. \end{aligned} \tag{4.8}$$

Here, the quadratures $x_{c,q} = (a^\dagger_{c,q} + a_{c,q})/\sqrt{2}$ and $y_{c,q} = i(a^\dagger_{c,q} - a_{c,q})/\sqrt{2}$ have been introduced. They fulfill the commutation relation $[x_c, y_q] = [y_c, -x_q] = i$ while all remaining commutators vanish. The form of the u_i and v_i indicate that the quadratures 'decouple'. The slow mode corresponds to x_c and its conjugate variable y_q while the fast mode is given by y_c and $-x_q$. This relates to the two quadratures $x_c = x_1$ and $y_c = x_2$ of Eq. (4.2). Close to threshold, we can describe the system by the relevant slow mode of the system, as it is in the case

of the classical case. We project the Liouvillian in Eq. (4.7) onto the subspace with $n_f = 0$ and obtain [32]

$$\mathcal{L} = \langle n_f = 0| \mathcal{L}_{\text{quad}} |n_f = 0\rangle = -\frac{(\bar{n} + \frac{1}{2})\gamma}{2} y_q^2 - i\frac{\epsilon - \gamma}{2} y_q x_c. \tag{4.9}$$

This Liouvillian describes a Fokker-Planck equation which is equivalent to the linearized ($\alpha = 0$) Langevin equation in Eq. (4.3) [33] .

When approaching the threshold at $\epsilon = \gamma$, it is essential to include a nonlinear potential V into the Hamiltionian. We examine two important cases. The first nonlinearity emerges due to a resonator that is driven by a voltage-biased Josephson junction. It reads $V_J = \frac{i\kappa\epsilon}{48}(a^\dagger a^3 - {a^\dagger}^3 a)$, see e.g. [30]. Here, $\kappa = 16\pi Z_0 G_Q$ is the effective fine-structure constant with the characteristic impedance Z_0 and the conductance quantum G_Q. The second nonlinearity corresponds to the generic nonlinearity in the rotating frame and describes the Duffing oscillator with $V_D = \chi\gamma a^\dagger a^\dagger a a$. Both potentials are characterized by a small parameter κ and χ. With either of the two potential, the full Liouvillian gains an additional term $\mathcal{L} = \mathcal{L}_{\text{quad}} + \mathcal{L}_V$ with $\mathcal{L}_V = -i(V_+ - V_-)$. Since the nonlinearities are small, we treat $\mathcal{L}_V$ as a perturbation. To obtain an effective model of the slow mode, we will project $\mathcal{L}_V$ onto the subspace with $n_f = 0$, see Ref. [6] for details. The effective nonlinearity of the Josephson oscillator can be obtained by first order perturbation theory, which results in a nonlinearity of the form $i\alpha y_q x_c^{m+1}$, with $\alpha = \kappa/48$ and $m = 2$. For the Duffing oscillator, it is necessary to include the second order since the first order vanishes due to the additional symmetry of the potential. Therefore,

$$\mathcal{L}_V \approx \langle n_f = 0| \mathcal{L}_V |n_f = 0\rangle - \sum_{n'_f \geq 1} \frac{\langle n_f = 0| \mathcal{L}_V |n'_f\rangle \langle n'_f| \mathcal{L}_V |n_f = 0\rangle}{\gamma n'_f}. \tag{4.10}$$

We obtain that $\alpha = \chi^2$ and $m = 4$. In total, the effective Liouvillian reads

$$\mathcal{L} = -\frac{(\bar{n} + \frac{1}{2})\gamma}{2} y^2 - i\frac{\epsilon - \gamma}{2} yx + \alpha i y x^{m+1}, \tag{4.11}$$

where we have dropped the subscripts 'q','c'. This corresponds to the classical Langevin equation in Eq. (4.3). This is due to the fact that the number of photons at threshold is very large, which enables a quasiclassical approach [5]. Finally, we rescale $y \mapsto p/x_*$ and $x \mapsto x_* q$ with $x_* = [(\bar{n} + 1/2)/\alpha]^{1/(m+2)}$ and obtain the universal Liouvillian of Ref. [6]

$$\mathcal{L} = -\frac{1}{\tau_*}\left(\frac{p^2}{2} + i\beta pq - ipq^{m+1}\right), \tag{4.12}$$

where $\tau_* = x_*^2/(\bar{n} + \frac{1}{2})\gamma$ is the correlation time and $\beta = \frac{1}{2}(\epsilon - \gamma)\tau_*$ the dimensionless distance to the threshold. We obtain the scaling $\tau_* \propto \alpha^{-2/(m+2)}$. This is the expected result from the equivalence of Langevin and Fokker-Planck equations. Note that it has the conventional definition of a $\mathcal{PT}$-symmetry, rather than

the Liouvillian symmetry that has been described in Sec. 3.3. This symmetry ensures that the spectrum is either real or has complex conjugate pairs, which is the property that follows from the hermiticity of the density matrix. Thus, the $\mathcal{PT}$-symmetry of the Liouvillian is inherited by the hermiticity constraint.

For both the Josephson and Duffing oscillator, additional terms appear when calculating the effective nonlinearity and are listed in the appendix of Ref. [6]. For example, terms like y^2 and iyx appear. They relate to a renormalization of noise and the threshold respectively. But since they scale with $\alpha \ll 1$ they can be neglected when we compare them to the terms that are already present in Eq. (4.9). Also, for the Josephson oscillator there is e.g. an additional term iy^3x and for the Duffing oscillator a term $-iyx^3$. But since we have that $x = x_* q$ and $y = p/x_*$, these terms are subleading in orders of x_*. The additional term of the Duffing oscillator has the wrong sign and does not stabilize the mode.

4.3 Radiation statistics

To access the radiation statistics of the system, we include a source term to the Liouvillian, as described in Sec. 2.3. It equals $\mathcal{L}_s = sf\mathcal{I}$, with the counting efficiency f, the counting field s, and the photon current operator $\mathcal{I} = \gamma a_+ a_-^\dagger$. Reducing this to the slow mode, we obtain $\mathcal{L}_s = sf\gamma(x + \frac{i}{2}p)^2/2$ [5, 32]. Since $x_* \gg 1$, the largest contribution of the counting term is given by $\mathcal{L}_s = f\gamma s x_*^2 q^2/2$. Therefore, the statistics are accessible by

$$\mathcal{L}_{\text{full}} = \mathcal{L} + \frac{sN_0}{\tau_*} q^2 \tag{4.13}$$

and the number of correlated photons at threshold $N_0 = f x_*^2 \tau_* \gamma/2$. The parameter scales with $N_0 \propto \alpha^{-4/(m+2)}$. The cumulants can be obtained by the generating function, see Sec. 2.3 and are given by

$$\langle\langle N^j \rangle\rangle = c_j N_0^j \frac{\tau}{\tau_*} \tag{4.14}$$

with universal numbers c_j, see [6]. To clarify, we obtain the factorial cumulants, see Sec. 2.3. The fact that $N_0 \gg 1$ implies that the difference between the normal and factorial cumulants, which is of order $1/N_0$, is small.

The stationary state is given by the solution of $\mathcal{L}P = \dot{P} = 0$ and characterizes the average photon current and $g^{(2)}(0)$. The latter is a measure for the amount of fluctuations and how likely it is to measure two photons at the same time. The results for these expressions can be found in Ref. [6] and are also shown in the next chapter when we compare the degenerate to the non-degenerate parametric oscillator. In the following, we turn to the higher order cumulants to compare the effective model to the full system given by the Lindblad equation. Also, we show present expressions that can be used to identify the microscopic parameters τ_* and N_0.

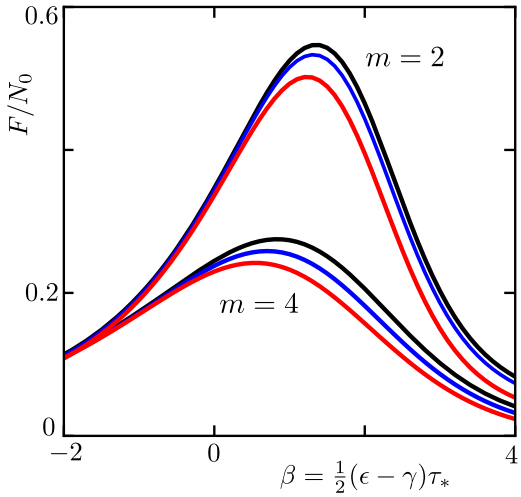

Figure 4.1: Comparison of the Fano factor of the effective model (black) compared to the full system for the values of the nonlinearity $\alpha = 10^{-3}$ (red) and $\alpha = 10^{-4}$ (blue) for the two different m. We see a good agreement between the full system and the effective model and that the deviation becomes smaller for $\alpha \to 0$. The deviation can also be eliminated by lowering the threshold and decreasing N_0.

First, we turn to the Fano factor $F = \langle\langle N^2 \rangle\rangle / \langle N \rangle = (c_2/c_1)N_0$. It parametrizes the number of correlated photons N_0. The expression F/N_0 has a universal form as a function of β and can be seen in Fig. 4.1. The black line expresses the Fano factor of the effective model and the blue and red line show the full system with for the values of the nonlinearity $\alpha = 10^{-3}$ (red) and 10^{-4} (blue). We see that below threshold, the Fano factor is equal for both exponents since the nonlinearity is not important yet. In the critical regime around threshold, we see two distinct curves but with similar characteristics, e.g. a peak close to threshold. For small driving strengths below the threshold, the value of F is 2 [30]. As the driving strength increases, F also increases. However, above threshold, the Poissonian statistics result in $F = 1$ creating a peak in between. The reason that the peak occurs slightly above threshold can be understood as follows: The universal Liouvillian in Eq. (4.12) can be seen as a particle in a potential $V(q) = -\beta q^2 + q^{m+2}$. Below threshold, $\beta < 0$, the potential is narrow and the particle does not have a lot of space to move around, which relates to small fluctuations. By increasing the driving, the potential gets broader which allows for on increase of the fluctuation and therefore the Fano factor. Slightly above threshold, $\beta > 0$, the potential turns into a double well. However, the separation of the minima of the potential, which scale with $\beta^{1/m}$, is small. Therefore, the particle gets even more room to move freely in the potential. Only when we are far above threshold, the separation of the minima is sufficient and the particle settles in one of the minima. This means that the second cumulant and therefore also the Fano factor decreases, and we obtain a peak slightly above threshold. In Fig. 4.1, we see that the full system approaches the effective model as α approaches 0. Furthermore, it is possible to eliminate

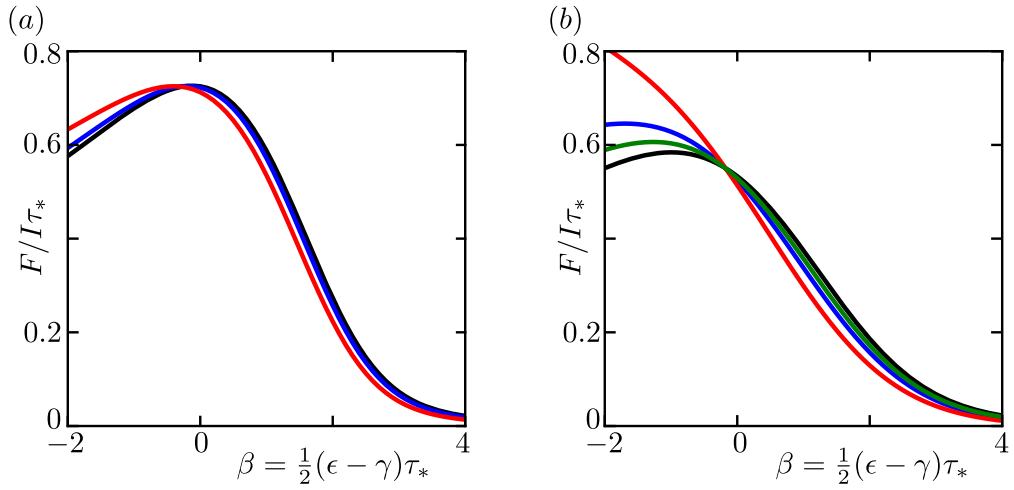

Figure 4.2: Comparison of the correlation time obtained by the effective model (black) compared to the full system. (a) Comparison for the Josephson oscillator ($m = 2$) with $\alpha = 10^{-3}$ (red) and $\alpha = 10^{-4}$ (blue). Again, a close agreement between the full system and the effective model described by the slow dynamics is shown. The deviation can be attributed to a lowering of the threshold. (b) Comparison for the Duffing oscillator ($m = 4$) with the same α values as before and an additional $\alpha = 10^{-5}$. Here, we see larger deviations that vanish as $\alpha \to 0$. The deviations are again given by a lowering of the threshold, this time with an additional increase of τ_*.

the deviations by decreasing the threshold, which effectively increases β, and a decrease of N_0. The second parameter is the characteristic timescale and can be identified by $F/I = (c_2/c_1^2)\tau_*$, where I is the average photon current. The universal expression $F/I\tau_*$ is shown in Fig. 4.2. The left panel displays the Josephson oscillator with $m = 2$. The deviation between the full system and the effective model is small and can be eliminated by lowering the threshold. The right panel depicts the Duffing oscillator with $m = 4$. We immediately notice that the full system shows a larger deviation to the result obtained by the effective model. There, an additional line in green with $\alpha = 10^{-5}$ has been added with a small deviation to the effective model. However, the deviation in this case can be lifted by a decrease of the threshold while additionally increasing τ_*. This can be again explained by the fact that some terms have been neglected in the derivation of the effective model for the Duffing oscillator. As discussed above, an additional term $-iy_q x_c^3 \sim -x_*^2$ appears in the effective model, which is subleading compared to $+iy_q x_c^5 \sim +x_*^4$. Due to its opposite sign, this term counteracts the stabilization, which results in the system taking a longer time to relax into the stationary state. As a consequence, the value of τ_* increases.

Chapter 5

Non-degenerate parametric oscillator

In the previous chapter, we have discussed the degenerate parametric oscillator and derived a universal model capturing the slow dynamics at the (classical) instability threshold. It has been shown that it accurately describes the dynamics by a comparison to the full system. Additionally, the occurring large number of photons makes a quasiclassical approach possible. In the following, the non-degenerate parametric oscillator is discussed, where two oscillators are parametrically driven at the sum of their resonance frequencies. Throughout this chapter, we refer to the oscillators as oscillator/resonator 'a' and 'b' or also first and second oscillator/resonator. We follow similar steps to the previous chapter. First, we quickly analyze the classical case. This allows us to point out some similarities and differences to the degenerate case and makes a better comparison of the quantum mechanical equivalent possible.

5.1 Classical Dynamics

The system contains two resonators with characteristic frequencies Ω_k and damping rates γ_k, where $k = a, b$. They are parametrically driven at the sum of their resonance frequencies, $\Omega_d = \Omega_a + \Omega_b$, and are described by the differential equation

$$\ddot{x}_k + \gamma_k \dot{x}_k + x_k[\Omega_k^2 + 2\sqrt{\Omega_a \Omega_b}\epsilon \sin(\Omega_d t)] = 0. \tag{5.1}$$

We follow the steps in Sec. 4.1 to obtain the differential equations in the rotating frame

$$\dot{A} = -\frac{\gamma_a}{2} A + \frac{\epsilon}{2} B^* \tag{5.2}$$

$$\dot{B} = -\frac{\gamma_b}{2} B + \frac{\epsilon}{2} A^* \tag{5.3}$$

expressed by the complex amplitudes A and B of resonator 'a' and 'b' respectively. For the following, we assume that the second resonator dissipates its energy much faster than resonator 'a', meaning that $\gamma_b \gg \gamma_a$. By comparison,

the second resonator equilibrates much faster and we can set $\dot{B} = 0$ in Eq. (5.3). Therefore, $B = (\epsilon/\gamma_b)A^*$ which we insert in Eq. (5.3) to obtain

$$\dot{A} = -\frac{\gamma_a}{2}\left(1 - \frac{\epsilon^2}{\gamma_a\gamma_b}\right)A. \tag{5.4}$$

We notice two things. Similar to the degenerate case, we obtain an instability, now at $\epsilon^2 = \gamma_a\gamma_b$. When the driving strength is close to this point, we have to include nonlinearities to cure the divergence. The difference to the degenerate case is that the driving does not couple to the complex conjugate of A anymore. This makes phase-insensitive amplification possible. All oscillations of resonator 'a' independent of their phase can be amplified.

Note that the oscillation amplitude of the second oscillator at threshold is given by $B = (\epsilon/\gamma_b)A^* = \sqrt{\gamma_a/\gamma_b}A^*$. Since $\gamma_b \gg \gamma_a$, the amplitude of oscillator 'b' is much smaller compared to the oscillations in oscillator 'a'. For the quantum system, $|B|^2$ relates to the number of photons inside the resonator. This means that the number of photons in resonator 'b' is a factor of γ_a/γ_b smaller than the photon number in resonator 'a'. Therefore, we can assume that the second resonator stays effectively in the ground state by comparison.

5.2 Effective Liouvillian

Below threshold and without dissipation, the quantum non-degenerate parametric oscillator can be described by the Hamiltonian [2]

$$H = \frac{i\epsilon}{2}\left(ab - a^\dagger b^\dagger\right), \tag{5.5}$$

given in the rotating frame where $a, a^\dagger$ and $b, b^\dagger$ are ladder operators obeying the canonical commutation relations. They correspond to the two resonators. Each oscillator is subject to single photon loss described by the jump operators

$$\mathcal{J}_{1,k} = \sqrt{\gamma_k(\bar{n}_k + 1)}\, k \quad \text{and} \quad \mathcal{J}_{2,k} = \sqrt{\gamma_k\bar{n}_k}\, k^\dagger, \tag{5.6}$$

with $k = a, b$ and $\bar{n}_k$ being the respective Bose-Einstein occupation. Now, we have gathered the necessary ingredients to diagonalize the Liouvillian. Since the matrices are quite large with $L \in \mathbb{C}^{8\times 8}$, we move the details about the diagonalization to the appendix A. First, we take a look at the eigenvalues of the Liouvillian that determine the time evolution. They are given by

$$\lambda_s = -\frac{1}{4}\left[\gamma_a + \gamma_b - \sqrt{4\epsilon^2 + (\gamma_a - \gamma_b)^2}\right], \tag{5.7}$$

$$\lambda_f = -\frac{1}{4}\left[\gamma_a + \gamma_b + \sqrt{4\epsilon^2 + (\gamma_a - \gamma_b)^2}\right], \tag{5.8}$$

where both eigenvalues are double degenerate. As in the case of the degenerate parametric oscillator above, we identify two modes. The first one, λ_s, corresponds to the slow mode and shows an instability at the classical value

$\epsilon^2 = \gamma_a\gamma_b$. The other, λ_f, is decaying for all values of ϵ and relates to the fast decaying mode with a decay rate of $(\gamma_a + \gamma_b)/2 \approx \gamma_b/2$ at threshold for $\gamma_b \gg \gamma_a$. This is already similar to the classical system, where resonator 'b' equilibrates much faster than the first oscillator. Also, there are again slow and fast timescales. Therefore, we can employ the same method that we have used for the degenerate oscillator to obtain a model of the relevant slow dynamics of oscillator 'a'. For the slow modes, we can approximate the Liouvillian by

$$\mathcal{L} \approx \lambda_s \left(v_1 u_1 + v_2 u_2\right), \tag{5.9}$$

where we have two number operators involved due to the degeneracy of the eigenvalue. For $\gamma_b \gg \gamma_a$ the number of photons in the second resonator are small compared to resonator 'a', as it has been pointed out in the previous section. We use this fact to assume that the second resonator is always in its ground state to obtain the effective model of resonator 'a'. In this regime, the Liouvillian of Eq. (5.9) reads

$$\mathcal{L} = -\frac{\left(\bar{n}_a + \bar{n}_b + 1\right)\gamma_a}{4}\,\frac{\boldsymbol{y}^2}{2} + \lambda_s i \boldsymbol{y}\cdot\boldsymbol{x}, \tag{5.10}$$

in terms of the quadratures $\boldsymbol{x} = (x_1, x_2)^T$ and the conjugate variables $\boldsymbol{y} = (y_1, y_2)^T$, with the canonical commutation relations $[x_i, y_j] = i\delta_{ij}$. This Liouvillian corresponds to a 2D-Fokker-Planck equation that relates to the classical expression in Eq. (5.4) with two differences. At first, we have included noise. Secondly, the prefactor of the second term does not match with the expression in Eq. (5.4). But, note that

$$\lambda_s = \lambda_s\lambda_f/\lambda_f \approx -2\lambda_s\lambda_f/\gamma_b = -\frac{\gamma_a}{2}\left(1 - \frac{\epsilon^2}{\gamma_a\gamma_b}\right) \tag{5.11}$$

close to threshold. Therefore, the effective Liouvillian represents again the classical differential equation. Again, the large photon number makes a quasi-classical approach possible.

Close to the instability, where $\epsilon \approx \sqrt{\gamma_a\gamma_b}$, it is necessary to include nonlinearities V into the Hamiltonian. The nonlinearities are characterized by the oscillator where we deal with two important case, the Josephson and the Duffing oscillator as in Sec. 4.2. The Josephson oscillator is implemented similar to above for the degenerate case. Now, the voltage bias tunes the driving frequency to match the sum of the resonant frequencies of the two resonators. This results in the nonlinearity [2]

$$V_J = \frac{i\kappa\epsilon}{16}\left(a^\dagger a^2 b - {a^\dagger}^2 b^\dagger a\right). \tag{5.12}$$

In general, there also appears another term in the same order of κ, but it includes higher orders of b-operators. Since the number of photons in resonator 'b' is much smaller than in resonator 'a', we only have to consider the expression in Eq. (5.12) that provides the largest contribution for this type of oscillator. The second nonlinearity given by the Duffing oscillator reads [34]

$$V_D = \chi\sqrt{2\gamma_a\gamma_b}\, a^\dagger a b^\dagger b, \tag{5.13}$$

and represents again the generic nonlinear potential in the rotating frame. Also in this case, there exist other possible potentials. For example, the Duffing nonlinearity that has been used for the degenerate oscillator, $V_{D,a} = \chi_a \gamma_a a^\dagger a^\dagger a a$. But it can be shown that this nonlinearity alone does not stabilize the mode anymore due to the phase-insensitive amplification. We have to include $V_{D,b} = \chi_b \gamma_b b^\dagger b^\dagger b b$ together with $V_{D,a}$ to stabilize the system. But since $V_{D,b}$ contains higher orders of b-operators it is less relevant than the expression in Eq. (5.13).

Again, we want to obtain an effective model for the slow 'a'-mode. As in the degenerate case in the previous chapter, we project the nonlinearities onto the subspace with $n_{f,1} = n_{f,2} = 0$ and afterwards adiabatically eliminate resonator 'b' that stays effectively in its ground state with $n_b = 0$. We start with the Josephson oscillator, where we have to use first order perturbation theory. First, we project the Keldysh superoperator b_c onto the slow mode and obtain that

$$\langle n_{f,i} = 0 |\, b_c \,| n_{f,i} = 0 \rangle = \sqrt{\frac{\gamma_a}{\gamma_b}} u_{s,1} + \sqrt{\frac{\gamma_a}{\gamma_b}} \gamma_a \frac{1 + \bar{n}_a + \bar{n}_b}{8\lambda_s} v_{s,2}, \tag{5.14}$$

using the definition of the ladder operators given in appendix A. Now, we use that the second resonator stays in the ground state, which results in an effective action for the first resonator. It reads

$$\langle n_b = 0 |\, u_{s,1} \,| n_b = 0 \rangle = -a_c^\dagger - \gamma_a \frac{1 + \bar{n}_a + \bar{n}_b}{8\lambda_s} a_q^\dagger, \tag{5.15}$$

$$\langle n_b = 0 |\, v_{s,2} \,| n_b = 0 \rangle = a_q^\dagger. \tag{5.16}$$

Therefore, we obtain the mapping $b_c \mapsto -\sqrt{\gamma_a/\gamma_b}\, a_c^\dagger$ for $\gamma_b \gg \gamma_a$. By the same method, we obtain that $b_q \mapsto \sqrt{\gamma_a/\gamma_b}\, a_q^\dagger$. Here, it becomes also apparent that terms with large orders in b can be safely neglected. The mapping can be then used to obtain the effective nonlinearity. Similar to the degenerate case, the amplitude of oscillation is large. Therefore, we will use a scaling with a charcteristic amplitude $r_* \gg 1$.[1] Then, the term with the smallest order in 'q' and highest order in 'c' provides the largest contribution, see Sec. 4.2. We obtain the effective nonlinearity

$$\mathcal{L}_{V_J} = \frac{\kappa \gamma_a}{8} (a_q a_c^\dagger - a_q^\dagger a_c) a_c^\dagger a_c = \frac{\kappa \gamma_a}{16} i \boldsymbol{y} \cdot \boldsymbol{x} |\boldsymbol{x}|^2. \tag{5.17}$$

By comparing to the degenerate case, we have obtained a nonlinearity in the form of $\alpha \gamma_a \boldsymbol{y} \cdot \boldsymbol{x} |\boldsymbol{x}|^m$. Therefore, the Josephson oscillator realizes the case of $\alpha = \kappa/16$ and again $m = 2$.

Next, we discuss the Duffing oscillator. The nonlinearity in terms of the Keldysh superoperators reads

$$\frac{i}{\chi\sqrt{2\gamma_a\gamma_b}} \mathcal{L}_{V_D} = a_c^\dagger a_c \left(b_q b_c^\dagger + b_q^\dagger b_c \right) + \left(a_q a_c^\dagger + a_q^\dagger a_c \right) b_c^\dagger b_c \tag{5.18}$$

[1] Since we have phase-insensitive amplification, both quadratures get amplified by the same amount. This is naturally rotational invariant, which is why we use the notation of r_*.

in leading order of the 'q'-operators. To obtain an effective description of the 'a'-mode it is necessary to perform second order perturbation theory. Then, the potential will be 'squared' which means that the 'q'-operators appear at least in the second half of Eq. (5.18). This is not the case for the first term, which is why we focus on this contribution. The effective potential can be obtained by

$$\mathcal{L}_{V_D} \approx -\sum_{n'_{f,1},n'_{f,2}\geq 1} \frac{2\left\langle n_{f,1}, n_{f,2}=0\right| \mathcal{L}_{V_D} \left|n'_{f,1}; n'_{f,2}\right\rangle \left\langle n'_{f,1}; n'_{f,2}\right| \mathcal{L}_{V_D} \left|n_{f,1}, n_{f,2}=0\right\rangle}{\gamma_b\left(n'_{f,1}+n'_{f,2}\right)}. \tag{5.19}$$

For the first term, $b_q b_c^\dagger$, this results in

$$\langle 0,0|\, b_q b_c^\dagger \,|1,0\rangle = -\sqrt{\frac{\gamma_a}{\gamma_b}} v_{s,2} \tag{5.20}$$

$$\langle 1,0|\, b_q b_c^\dagger \,|0,0\rangle = -\sqrt{\frac{\gamma_a}{\gamma_b}} u_{s,2} - \frac{\gamma_a}{\gamma_b}\frac{(1+\bar{n}_a+\bar{n}_b)\sqrt{\gamma_a\gamma_b}}{8\lambda_s} v_{s,1} - \left(\frac{\gamma_a}{\gamma_b}\right)^{\frac{3}{2}} \frac{(1+\bar{n}_a+\bar{n}_b)}{4} v_{s,2}. \tag{5.21}$$

Again, we use that the second resonator is in the ground state. We obtain the mapping

$$b_q b_c^\dagger \mapsto \frac{\gamma_a}{\gamma_b}\, a_q^\dagger a_c + \frac{\gamma_a^2}{\gamma_b^2}\frac{1+\bar{n}_a+\bar{n}_b}{4} {a_q}^2. \tag{5.22}$$

We neglect the second term since it is of quadratic order in 'q' and also quadratic in $\gamma_a/\gamma_b \ll 1$. For the other term, we obtain

$$b_q^\dagger b_c \mapsto -\frac{\gamma_a}{\gamma_b}\, a_q a_c^\dagger + \frac{\gamma_a^2}{\gamma_b^2}\frac{1+\bar{n}_a+\bar{n}_b}{4} {a_q^\dagger}^2 \tag{5.23}$$

by the same procedure. Again, we drop the second term and obtain the effective nonlinearity

$$\mathcal{L}_{V_D} = \chi^2 \frac{\gamma_a^2}{\gamma_b}(a_q a_c^\dagger - a_q^\dagger a_c)(a_c^\dagger a_c)^2 = \chi^2 \frac{\gamma_a^2}{\gamma_b} i\boldsymbol{y}\cdot\boldsymbol{x}|\boldsymbol{x}|^4. \tag{5.24}$$

It is once more of the form $\alpha i\boldsymbol{y}\cdot\boldsymbol{x}|\boldsymbol{x}|^m$. This time with $\alpha = \chi^2\gamma_a/\gamma_b$ and $m = 4$.

In total, we obtain the universal Liouvillian

$$\mathcal{L} = -\frac{1}{\tau_*}\left(\frac{\boldsymbol{p}^2}{2} + i\beta\boldsymbol{p}\cdot\boldsymbol{q} - i\boldsymbol{p}\cdot\boldsymbol{q}|\boldsymbol{q}|^m\right), \tag{5.25}$$

where we have used the rescaling $x_i = r_* q_i$ and $y_i = p_i/r_*$ with the characteristic amplitude $r_* = [(1+\bar{n}_a+\bar{n}_b)/4\alpha]^{1/(m+2)}$. The characteristic timescale is given by $\tau_* = 4r_*^2/(1+\bar{n}_a+\bar{n}_b)\gamma_a$. The dimensionless distance to threshold is determined by $\beta = \frac{1}{2}(\epsilon^2/\gamma_a\gamma_b - 1)\tau_*\gamma_a$. We obtain the same universal scaling of $\tau_* \sim \alpha^{-2/(m+2)}$ as for the degenerate parametric oscillator. The main differences are the details of the microscopic parameters and that the universal Liouvillian is now a 2D-Fokker-Planck equation for the probability distribution P with

$\dot{P} = \mathcal{L}P$. Note that this universal Liouvillian also enjoys a $\mathcal{PT}$-symmetry that is inherited by the hermiticity of the density matrix. Additionally, the Liouvillian has a rotational invariance. The Liouvillian commutes with the angular momentum operator $L_z = q_1 p_2 - q_2 p_1$, which is the generator for rotations in 2D. This property is addressed in the next chapter when we move to the task of solving the Liouvillian.

As a last step of this section, we discuss the source term for the photon counting that we have to add to the Liouvillian to access the radiation statistics. It reads $\mathcal{L}_s = sf\mathcal{I}$, with the counting efficiency f and the photon current operator of resonator 'a' given by $\mathcal{I} = \gamma_a a_+ a_-^\dagger$. For the slow mode and in leading order of r_*, we obtain

$$\mathcal{L}_s = \frac{sf\gamma_a \Gamma_b r_*^2}{2}(q_1^2 + q_2^2) \overset{\gamma_b \gg \gamma_a}{\approx} \frac{sf\gamma_a r_*^2}{2}(q_1^2 + q_2^2) = \frac{sN_0}{\tau_*}(q_1^2 + q_2^2), \tag{5.26}$$

with the number of correlated photons $N_0 = f\gamma_a r_*^2 \tau_*/2 \sim \alpha^{-4/(m+2)}$. Again, the scaling of the nonlinearity is the same as for the degenerate parametric oscillator. The result for the counting term in Eq. (5.26) can also be obtained by the following argument: In general, we have that $a_+ a_-^\dagger = \frac{1}{2}(x_1 + \frac{i}{2}y_1)^2 + \frac{1}{2}(x_2 + \frac{i}{2}y_2)^2$. Since both x_1 and x_2 get amplified, we can approximate it by the leading order $a_+ a_-^\dagger \approx \frac{1}{2}\left(x_1^2 + x_2^2\right)$, where $x_i = r_* q_i$, which equals the expression in Eq. (5.26).

5.3 Solving the Liouvillian

In the previous section, we have derived the universal Liouvillian for the non-degenerate parametric oscillator in the limit $\gamma_b \gg \gamma_a$. Due to the involved nonlinearities, we have limited options to obtain analytical results for the radiation statistics. Therefore, we first show how to efficiently solve the Liouvillian (numerically).

5.3.1 Laguerre polynomials

We start by employing the rotational invariance of the Liouvillian and express it in polar coordinates by the radius $r^2 = q_1^2 + q_2^2$ and the angle $\tan(\varphi) = q_2/q_1$. Also, we choose a separation Ansatz for the probability distribution $P(q_1, q_2, = P(r, \varphi) = e^{im_l \varphi} R(r)$, with $m_l \in \mathbb{Z}$ being an eigenvalue of the angular momentum operator, and additionally $R(r) = u(r)/r$. This choice eliminates the φ dependence of the Liouvillian due to the rotational symmetry. Whenever an integral over the probability distribution is required, as it is the case for the normalization of $P(r, \varphi)$ or the calculation of expectation values, we can express it by $u(r)$, since

$$\int dq_1 \int dq_2 P(q_1, q_2) = \int d\varphi \int dr\, r P(r, \varphi) = \underbrace{\int d\varphi e^{im_l \varphi}}_{\delta_{m_l,0}} \int dr\, u(r). \tag{5.27}$$

The corresponding Liouvillian for $u(r)$ is given by

$$\mathcal{L} = -\frac{1}{\tau_*}\left[\frac{p^2}{2} + i\beta pr - ip\left(r^{m+1} - \frac{1}{2r}\right) + \frac{m_l^2}{2r^2}\right], \tag{5.28}$$

with $p = -i\partial_r$ and the canonical commutation relation $[r, p] = i$. [2] Note that the Liouvillian is independent of the sign of m_l. Therefore, we use $l = |m_l|$ for the following. Also, the stationary probability distribution is given by the 'state' with $l = m_l = 0$. This can be identified in two ways. First, the normalization of the stationary state given in Eq. (5.27) requires $m_l = 0$. Also, when applying the trace (left eigenstate to eigenvalue $\lambda = 0$, see Sec. 2.2.3) on the Liouvillian, it is only vanishing for $l = m_l = 0$. The stationary state will be discussed more detailed in the next section.

The Liouvillian in Eq. (5.28) seems to be not well-defined at $r = 0$. Because of this and that the position operator is not invertible, we are not able to simulate the Liouvillian in this form. This means that we need to do further transformations to obtain a suitable form of the Liouvillian. We continue by choosing the Ansatz $u(r) = g(r)f(r)$ to eliminate the first order derivatives of $f(r)$. To be more precise on what this means, we insert the Ansatz in Eq. (5.28). This results in a variety of terms including $f'(r)D(g(r), g'(r))$. Now, we want $D(g(r), g'(r)) = 0$, such that the first derivative of $f(r)$ does not appear in the Liouvillian anymore. This is a differential equation that is solved by $g(r) = C\sqrt{r}\exp\left[\beta r^2/2 - r^{m+2}/(m+2)\right]$, with an arbitrary constant C. Then, the Liouvillian is a Schrödinger-like-equation of the form

$$\begin{aligned}\mathcal{L} &= -\frac{1}{\tau_*}\left(\frac{p^2}{2} + V_{\text{eff}}(r)\right) \\ &= -\frac{1}{\tau_*}\left(\frac{p^2}{2} - \frac{\frac{1}{4} - l^2}{2r^2} + \beta + \frac{\beta^2}{2}r^2 - \frac{m+2}{2}r^m - \beta r^{m+2} + \frac{1}{2}r^{2m+2}\right),\end{aligned} \tag{5.29}$$

with an effective potential $V_{\text{eff}}(r)$. We do not focus on the equation in this form since it does not resolve the issue at $r = 0$ but it is most likely to obtain further insights when analyzing this effective potential.

The first two terms in Eq. (5.29) are part of an already known differential equation [35]. It reads

$$\frac{1}{2}v'' + \frac{\frac{1}{4} - l^2}{2r^2}v = -\left(2n + l + 1 - \frac{1}{2}r^2\right)v \tag{5.30}$$

and is solved by $v(r) = r^{l+1/2}\exp\left(-r^2/2\right)L_n^{(l)}(r^2)$, with generalized Lagurre polynomials $L_n^{(l)}(r^2)$. Therefore, we choose the Ansatz $f(r) = \sum_n c_n v(r)$ and are able to use the orthogonality relation of the Laguerre polynomials

$$\int_0^\infty dx\, x^l e^{-x} L_n^{(l)}(x) L_m^{(l)}(x) = \frac{(n+l)!}{n!}\delta_{nm}, \tag{5.31}$$

[2] Strictly speaking, this choice of p_r is not Hermitian. Since the formalism here does not rely on hermiticity, we can ignore this fact.

with $x = r^2$, to obtain a Liouvillian for the coefficients c_n. For a given l, it reads

$$\mathcal{L} = -\frac{1}{\tau_*}\left(2n + l + 1 + \beta + \frac{\beta^2 - 1}{2}r^2 - \frac{m+2}{2}r^m - \beta r^{m+2} + \frac{1}{2}r^{2m+2}\right) \quad (5.32)$$

and the $1/r$-'problem' is resolved. In this form, we are able to perform an efficient numerical evaluation of the Liouvillian. To summerize the results of this section up to here, we have started with a two-dimensional coupled partial differential equation in (5.25). By employing the rotational invariance, we have been able to express the Liouvillian by the radial component r and have obtained a one dimensional differential equation, that resembles a simple eigenvalue problem. We obtain the eigenstates to an eigenvalue λ_i of the Liouvillian by

$$P_i(r, \varphi) = e^{im_l\varphi}\sum_n c_n r^l e^{\frac{\beta-1}{2}r^2 - \frac{1}{m+2}r^{m+2}} L_n^{(l)}(r^2), \quad (5.33)$$

where the c_n can be determined from Eq. (5.32). To evaluate this expression, we need to determine the matrix elements of r^2. The Liouvillian only contains higher orders of r^2 since m is in general any positive and even number. The photon counting operator is given by r^2 as well, see Eq. (5.26). The matrix elements are given by the recurrence formula of the generalized Laguerre polynomials

$$\begin{aligned} r^2 L_n^{(l)}(r^2) = &-\sqrt{(n+1)(n+l+1)}L_{n+1}^{(l)}(r^2) - \sqrt{n(n+l)}L_{n-1}^{(l)}(r^2) \\ &+ (2n + l + 1)L_n^{(l)}(r^2), \end{aligned} \quad (5.34)$$

where we have normalized the Laguerre polynomials according to Eq. (5.31). In this form, r^2 is Hermitian, and therefore the Liouvillian is Hermitian as well. Since the Fock-basis is not necessarily Hermitian, see Sec. 2.2.3, we may also choose to move the normalization into the left eigenbasis or even into the weighting function $x^l e^{-x}$ of the normalization itself. But throughout the steps above, we have transformed the Liouvillian in multiple ways, which have also affected the spectrum. For example, also the Liouvillian of the Schrödinger-like-equation in Eq. (5.29) can be implemented as a Hermitian operator. Because of this, we 'lose' the complex conjugate pairs in the spectrum of $\mathcal{L}$. Furthermore, we have pointed out in Sec. 2.2.3 that the trace preservation of the Lindblad equation is the key ingredient to work out the Fock-structure of the formalism. It guarantees that the eigenvalue $\lambda = 0$ exists, and therefore also the stationary state. For example, the starting expression of the universal Liouvillian in Eq. (5.25) is clearly trace preserving, because the p_i are 'q'-operators in the superoperator formalism that encode exactly this property. Whether the Liouvillian is still trace preserving in the Schrödinger-like form of Eq. (5.29) or also in Eq. (5.32) is not clear anymore. Therefore, it is necessary to look out for an appropriate choice of r^2 that fulfills two properties on the spectrum of $\mathcal{L}$. First, there should not be any eigenvalues with a positive real part, since the system would be unstable in this case. Second, there should be an eigenvalue $\lambda = 0$ that corresponds to trace preservation and also the stationary state. If we choose

that the normalization of the Laguerre polynomials is e.g. shifted into the integral measure, we actually lose both of these properties. Therefore, we work with the choice of r^2 given in Eq. (5.34). With the proper tools prepared, we are now able to obtain the radiation statistics of the non-degenerate parametric oscillator, which is discussed in the last section of this chapter. But first, we are going to discuss another method to numerically solve the Liouvillian based on the 2D-harmonic oscillator.

5.3.2 2D-Harmonic oscillator

For the degenerate case where the system has been described by a 1D-Fokker-Planck equation, the eigenstates of the Liouvillian are given by a superposition of Hermite-functions. The Liouvillian for the non-degenerate oscillator resembles a 2D-Fokker-Planck equation, and also the expression in Eq. (5.9) is related to the isotropic two-dimensional harmonic oscillator. Therefore, we discuss quickly how it is possible to solve the Liouvillian using the knowledge about the two-dimensional harmonic oscillator. There, it is also possible to use the rotational symmetry of the Hamiltonian to simultaneously diagonalize the angular momentum operator L_z. Then, instead of having excitations n_x and n_y that relate to excitation in the different directions x and y, it is possible to describe the system by right and left rotating quanta n_r and n_l. The second quantized, dimensionless Hamiltonian is given by

$$H = a_1^\dagger a_1 + a_2^\dagger a_2, \tag{5.35}$$

with the ladder operators $a_i = (q_i + ip_i)/\sqrt{2}$ that fulfil the canonical commutation relations $[q_i, p_j] = i\delta_{ij}$ and $[a_i, a_j^\dagger] = \delta_{ij}$. The angular momentum is given by $L_z = q_1 p_2 - q_2 p_1 = i(a_1 a_2^\dagger - a_1^\dagger a_2)$, with $L_z^\dagger = L_z$. Since L_z commutes with the Hamiltonian and both are Hermitian, we are able to diagonalize L_z as well. This is done by introducing new ladder operators given by $a_r = (a_1 + ia_2)/\sqrt{2}$ and $a_l = (a_1 - ia_2)/\sqrt{2}$ which relate to rotating quanta. While the former corresponds to clockwise rotations, the a_l relate to counter-clockwise rotations. In this basis, we obtain

$$H = a_l^\dagger a_l + a_r^\dagger a_r \quad \text{and} \quad L_z = a_l^\dagger a_l - a_r^\dagger a_r. \tag{5.36}$$

The eigenvalues are given by $n = n_l + n_r$ and $m_l = n_l - n_r$ respectively and therefore $n_l = (n + m_l)/2$ and $n_r = (n - m_l)/2$. Note that H still counts the number of total excitations, while L_z counts the difference between the number of counterclockwise and clockwise rotations. It measures the angular momentum m_l in the system with $m_l = -n, -n+2, ..., n-2, n$ given a fixed n.

They act on an eigenstate $|n, m_l\rangle$ with

$$\begin{aligned} a_l |n, m_l\rangle &= \sqrt{\frac{n+m_l}{2}} |n-1, m_l-1\rangle , \\ a_l^\dagger |n, m_l\rangle &= \sqrt{\frac{n+m_l}{2}+1} |n+1, m_l+1\rangle , \\ a_r |n, m_l\rangle &= \sqrt{\frac{n-m_l}{2}} |n-1, m_l+1\rangle , \\ \text{and} \quad a_r^\dagger |n, m_l\rangle &= \sqrt{\frac{n-m_l}{2}+1} |n+1, m_l-1\rangle . \end{aligned} \tag{5.37}$$

When a counterclokwise rotating quant is annihilated, the total number n as well as the angular momentum m_l are decreased by 1. When a clockwise rotating quant is annihilated, the total number decreases but the angular momentum increases since the difference between counter-clockwise and clockwise rotations increases.

Given this algebra, we are able to solve the Liouvillian due to the rotational invariance. We choose the Ansatz that the eigenstates of the Liouvillian are given by a linear combination of the eigenfunctions of the 2D-harmonic oscillator. To this end, we need to determine the action of three terms in this basis: $\boldsymbol{p}^2$, $i\boldsymbol{p}\cdot\boldsymbol{q}$ and $\boldsymbol{q}^2$. We obtain

$$\boldsymbol{p}^2 = a_l^\dagger a_l + a_r^\dagger a_r - a_l^\dagger a_r^\dagger - a_l a_r + 1, \tag{5.38}$$

$$i\boldsymbol{p}\cdot\boldsymbol{q} = a_l a_r - a_l^\dagger a_r^\dagger + 1, \quad \text{and} \tag{5.39}$$

$$\boldsymbol{q}^2 = a_l^\dagger a_l + a_r^\dagger a_r + a_l^\dagger a_r^\dagger + a_l a_r + 1. \tag{5.40}$$

Note that each term does not change the angular momentum m_l. Since we are interested in the radiation statistics of the stationary state, we set $m_l = 0$.

5.4 Radiation statistics

In this final section, we show the resulting radiation statistics for the non-degenerate parametric oscillator. Since the number of photons is large, the difference between the factorial cumulants and the normal cumulants at threshold is small. They have the same form as above: $\langle\langle N^j \rangle\rangle = c_j N_0 \tau/\tau_*$ with universal numbers c_j which are listed in Table 5.1. The cumulants and expressions derived from them have a universal form as a function of β. Before we show them, we turn to the stationary state where some analytical results can be obtained.

5.4.1 Stationary state

The stationary state is characterized by the probability distribution $P(r)$ [3] that is connected to the eigenvalue $\lambda = 0$ and solves the differential equation $\dot{P} = \mathcal{L}P = 0$. It is given by $P(r) \sim \exp\big(\beta r^2 - 2r^{m+2}/(m+2)\big)$. From this, we

[3] We have that $l = 0$. Therefore, the probability distribution is independent of φ.

m	c_1	c_2	c_3	c_4
2	$\sqrt{2/\pi} \approx 0.798$	0.176	0.0462	−0.00421
4	$3^{1/3}\Gamma(\frac{2}{3})/\Gamma(\frac{1}{3}) \approx 0.729$	0.0942	0.00375	−0.00622

Table 5.1: Coefficients of the photon counting at threshold

first determine the average photon current. The photon current is defined via $I = \frac{1}{2} f \gamma_a r_*^2 (q_1^2 + q_2^2) = \frac{1}{2} f \gamma_a r_*^2 r^2$. The expectation value is given by averaging over the stationary probability distribution. We obtain that

$$\langle r^2 \rangle = \beta + \sqrt{\frac{2}{\pi}} \frac{e^{-\frac{\beta^2}{2}}}{1 + \mathrm{Erf}(\frac{\beta}{\sqrt{2}})} \tag{5.41}$$

for $m = 2$ where $\mathrm{Erf}(x)$ is the Gaussian error function. For $m = 4$, the expectation value reads

$$\langle r^2 \rangle = \frac{4\pi \mathrm{Ai}'(\beta) + 6\beta\, \mathrm{F}(a_1 = 1, b_1 = \frac{2}{3}, b_2 = \frac{4}{3}, \frac{\beta^3}{9})}{4\pi \mathrm{Ai}(\beta) + 3\beta^2\, \mathrm{F}(a_1 = 1, b_1 = \frac{4}{3}, b_2 = \frac{5}{3}, \frac{\beta^3}{9})}, \tag{5.42}$$

with the Airy-function $\mathrm{Ai}(x)$ and the generalized hypergeometric function $\mathrm{F}(\boldsymbol{a}, \boldsymbol{b}, z)$. For definitions, see e.g. [36, 37]. The results for the average photon current can be seen in Fig. 5.1. There, we compare them (black lines) to the case of the

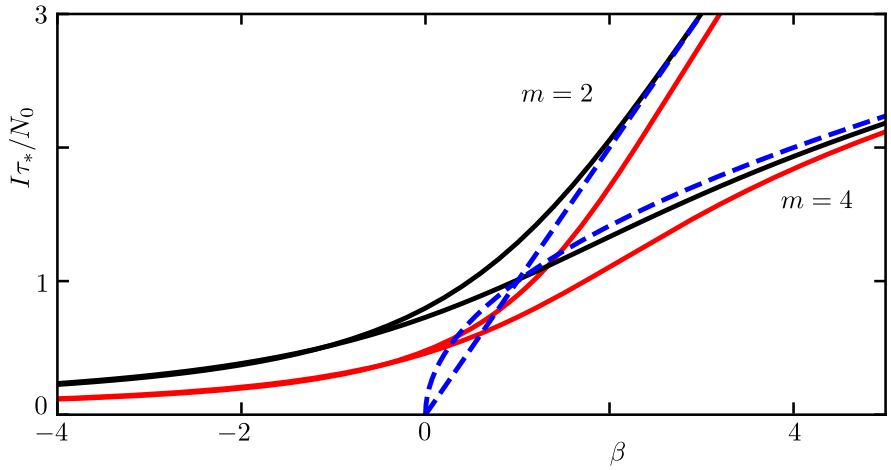

Figure 5.1: Average photon current of the non-degenerate (black) and degenerate (red) parametric oscillator compared to each other and the classical expectation $\beta^{2/m}$ (blue dashed). Below threshold, the two parametric oscillators show a deviation that is due to the fact that we are in the regime of $\gamma_b \gg \gamma_a$. Close to threshold, the current 'splits' into the two different cases $m = 2$ and 4. Above threshold, they converge to the classical expectation.

degenerate oscillator (red lines), as well as the classical expectation $1/\beta^{2/m}$ for both $m = 2$ and 4 (blue dashed lines). Above threshold, the two different

cases of m converge to the classical value. Therefore, both models recreate the correct classical behavior above threshold. Below threshold the non-degenerate and degenerate case show a small, at first sight unexpected, deviation since photon counting statistics belong to the same universality class [5]. But here, we have gone into a limit ($\gamma_b \gg \gamma_a$) where the second oscillator is 'eliminated'. In this limit, the universality is not present anymore that is also depicted here. In particular, we see that the counting statistics are different, although they show the same scaling on the nonlinearity $N_0/\tau_* \sim \alpha^{-2/(m+2)}$.

We further look at the second order coherence $g^{(2)}(\tau = 0) = \langle r^4\rangle/\langle r^2\rangle^2$. Generally, the second order coherence $g^{(2)}(\tau)$ is a measure for the correlation of an emitted photon after a time τ given a previously emitted photon. In general, there are three possible cases. When the radiation is uncorrelated, we have that $\langle r^4\rangle = \langle r^2\rangle^2$ and therefore $g^{(2)} = 1$. For $g^{(2)} > 1$ it is likely to measure another photon, which is called photon bunching. And for $g^{(2)} < 1$, the radiation is called antibunched. At threshold ($\beta = 0$), we obtain $g^{(2)}(0) = \pi/2 \approx 1.57$ for $m = 2$ and for $m = 4$ we get $g^{(2)}(0) = \Gamma(\frac{1}{3})/\Gamma(\frac{2}{3})^2 \approx 1.46$. In both cases we have that $g^{(2)}(0) > 1$ and the emitted photons are therefore bunched. As for the average photon current, it is possible to evaluate the expression $g^{(2)}(0) = \langle r^4\rangle/\langle r^2\rangle^2$ for all values of β. But the expressions given in Eq. (5.41) and (5.42) prove that analytical expressions do not necessarily provide further insights. Therefore, we 'just' show the result in Fig. 5.2. We see that the radiation is bunched for all driving strengths. Above threshold, $g^{(2)}(0)$ approaches 1. This means that the emission of photons becomes uncorrelated. This is due to the fact that for large β, we reach the classical regime where the radiation statistics become Poissonian.

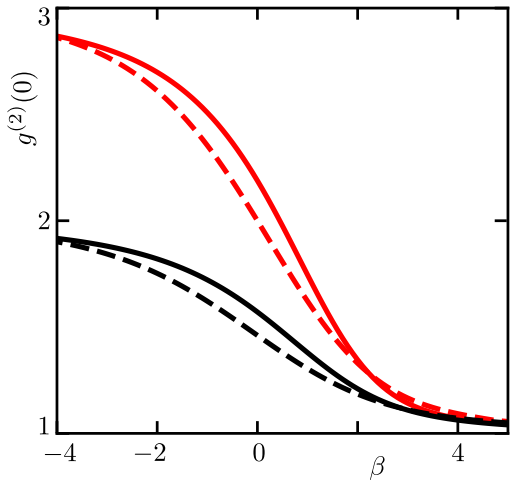

Figure 5.2: Comparison of the value of $g^{(2)}(0)$ for the different cases of the (non)-degenerate parametric oscillator in (black) red and for $m = 2(4)$ in solid (dashed) lines. For all values of β, $g^{(2)}(0)$ is larger than 1, indicating that the radiation is bunched. Above threshold, the value approaches 1 since we reach the classical regime where the photon statistics are Poissonian and the photon emission is uncorrelated.

5.4.2 Higher order cumulants

In the previous part, we have dealt with the stationary probability distribution of the system. Here, we also consider the dynamics of the system that are expressed in the higher order cumulants. To gain access to the higher cumulants, we need to add the source term to the Liouvillian and determine the generating function. As in Sec. 4.3, we start with expressions that can be used to identify the microscopic parameters.

We start with the Fano factor $F = \langle\langle N^2 \rangle\rangle / \langle N \rangle = (c_2/c_1)N_0$ that relates to the number of correlated photons N_0. The reduced expression $F/N_0 = c_2/c_1$ has a universal form that can be seen in Fig. 5.3.

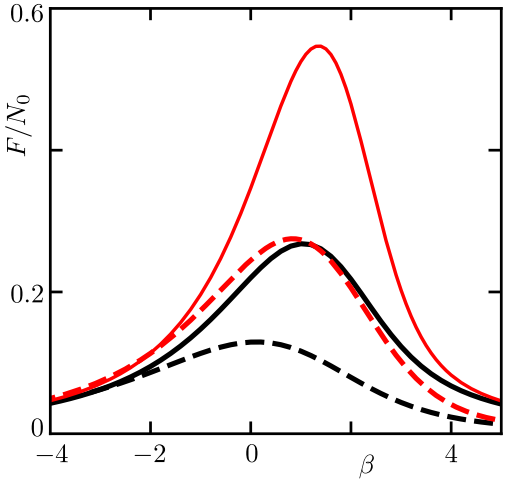

Figure 5.3: Fano factor of the non-degenerate (black) compared to the degenerate (red) case for the different exponents $m = 2(4)$ in solid (dashed) lines. The universal form of F/N_0 is very similar for all cases, with a peak close above threshold. For both the non-degenerate and degenerate parametric oscillator, the Fano factor of $m = 4$ is smaller than the case $m = 2$.

The black lines represent the non-degenerate parametric oscillator, while the red lines belong to the degenerate case for comparison. The different exponents $m = 2$ and 4 are given in solid and dashed lines respectively. This form of presentation will also be used for the following expressions. We see that for each case the curves have a very similar form with a peak close above threshold. How it is possible to think of this has been explained in Sec. 4.3 for the degenerate parametric oscillator. Here, the thought is similar. The only difference is that we have a particle moving in the effective rotational symmetric potential $V(r) = -\beta r^2 + r^{m+2}$ with $r \in [0, \infty)$. Below threshold, the particle is constrained in the minima of the 'parabola' at $r = 0$. When the system is driven above threshold, $\beta > 0$, the potential turns into a 'Sombrero'. For small positive β the well of the potential is not deep enough to keep the particle in the just emerged minima. Only for stronger driving, the particle is constrained. Therefore, the Fano factor shows again a peak (slightly) above threshold. The peaks of the Fano factor for the non-degenerate case occur at $F = 0.265\, N_0$,

$\beta = 0.8$ for $m = 2$ and at $F = 0.129\,N_0$, $\beta = 0.2$ for $m = 4$. For comparison, the peaks for the degenerate parametric oscillator are at $F = 0.547\,N_0$, $\beta = 1.4$ for $m = 2$ and at $F = 0.275\,N_0$, $\beta = 0.8$ for $m = 4$.

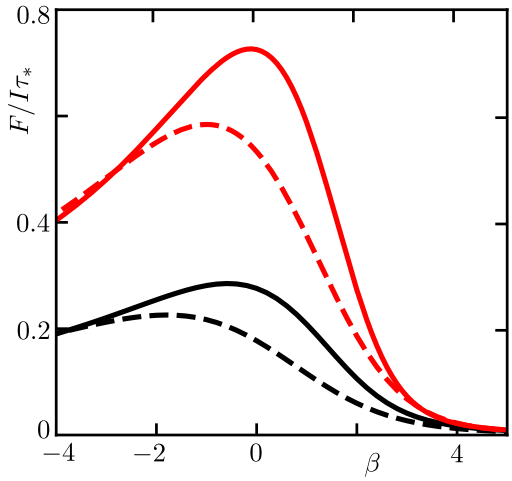

Figure 5.4: Correlation time of the non-degenerate (black) compared to the degenerate (red) case for the different exponents $m = 2(4)$ in solid (dashed) lines. Again, all cases show very similar behavior as a function of β with a peak close to threshold. Above threshold, the system reaches the classical regime, where the radiation statistics are Poissonian and the emission events are uncorrelated. Therefore, the correlation time approaches 0 which is also depicted here.

The correlation time τ_* is given by the ratio $F/I = (c_2/c_1^2)\tau_*$ and is displayed in Fig. 5.4. Again, we see very similar behavior in both systems and for both exponents m. First, it increases when we approach the threshold. The influence of the nonlinearity in this regime is small. The correlation time of the linearized theory is given by $\tau_* \propto 1/\beta$. This means that the timescale significantly increases close to threshold. Then, the nonlinearity becomes important which stabilizes the system. This cures the divergence and leads to a peak around threshold. For even larger driving strengths, we reach the Poissonian regime. There, the emitted radiation is uncorrelated, meaning that τ_* approaches 0. For the non-degenerate case, we obtain a peak at $F/I = 0.285\,\tau_*$, $\beta = -0.6$ for $m = 2$ and $F/I = 0.226\,\tau_*$, $\beta = -1.8$ for $m = 4$. The degenerate case shows peaks at $F/I = 0.726\,\tau_*$, $\beta = -0.1$ for $m = 2$ and $F/I = 0.584\,\tau_*$, $\beta = -1$ for $m = 4$.

The correlation time determines the width of the second order coherence $g^{(2)}(\tau)$. We can approximate the coherence by

$$g^{(2)}(\tau) = 1 + \frac{\lambda}{2}\frac{F}{I}e^{-\lambda|\tau|}\,, \tag{5.43}$$

where λ is the smallest eigenvalue (besides $\lambda = 0$) of $-\mathcal{L}$. It has the value $\lambda \approx 3.99/\tau_*$ for $m = 2$ and $\lambda \approx 4.84/\tau_*$ for $m = 4$. When we compare this

expression to numerics, it shows just a small deviation at $\tau = 0$. Even there, the deviation is around 1 or 2 percent for $m = 2, 4$ respectively. Therefore, this expression is an excellent approximation of the second order coherence which can also be seen in Fig. 5.5. There, the black lines are given by numerics and the red dotted lines by the expression in Eq. (5.43). Finally, we show

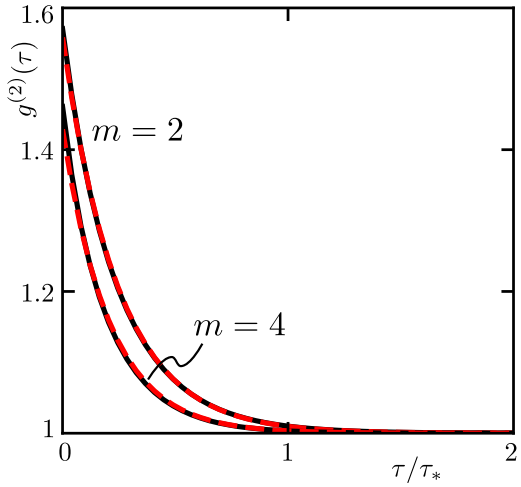

Figure 5.5: Comparison of the approximated second order coherence (red dashed) to the numerical result (black solid). The expression in Eq. (5.43) provides an excellent approximation for the second order coherence. The deviation at $\tau = 0$ is around 1 or 2 percent for $m = 2$ and 4 respectively. Note that the radiation becomes uncorrelated after a time $\tau = \tau_*$, since $g^{(2)}(\tau) \approx 1$, which gives τ_* its name.

the universal ratio $u = \langle N\rangle\langle\!\langle N^3\rangle\!\rangle/\langle\!\langle N^2\rangle\!\rangle^2 = c_1c_3/c_2^2$ that is independent of the microscopic parameters N_0 and τ_*. It is motivated by the form of the cumulants given explicitly in Eq. (4.14) or also in the beginning of this section. The ratio is universal since the microscopic parameters of the system drop out. Therefore, only the universal number c_j are left over. Of course, there exist a variety of universal ratios such as $u' = \langle N\rangle\langle\!\langle N^4\rangle\!\rangle/\langle\!\langle N^2\rangle\!\rangle\langle\!\langle N^3\rangle\!\rangle = c_1c_4/c_2c_3$ or $u'' = \langle N\rangle^2\langle\!\langle N^4\rangle\!\rangle/\langle\!\langle N^2\rangle\!\rangle^3 = c_1^2c_4/c_2^3$. But all of them include cumulants beyond the third one. Therefore, we focus on the simplest expression given by the ratio of the first three cumulants shown in Fig. 5.6 with the black lines for the non-degenerate parametric oscillator and in red for the degenerate case. The exponents $m = 2$ and 4 are shown in solid and dashed lines respectively. Far below threshold, both the non-degenerate and degenerate parametric oscillator start at the finite value 3 that follows from the universality derived in Ref. [5]. Then, it gradually decreases and the non-degenerate and degenerate case show a deviation at threshold. As it has been pointed out above, the radiation of the two systems is not expected to be the same in the critical regime anymore, so the deviation is not surprising. The ratio also becomes negative above threshold, where the zero point crossings occur at $\beta = 1.085\,(0.265)$ for the non-degenerate and at $\beta = 1.402\,(0.998)$ for the degenerate case for $m = 2(4)$. Since the first two cumulants are always positive, this characteristic is inherited by the third

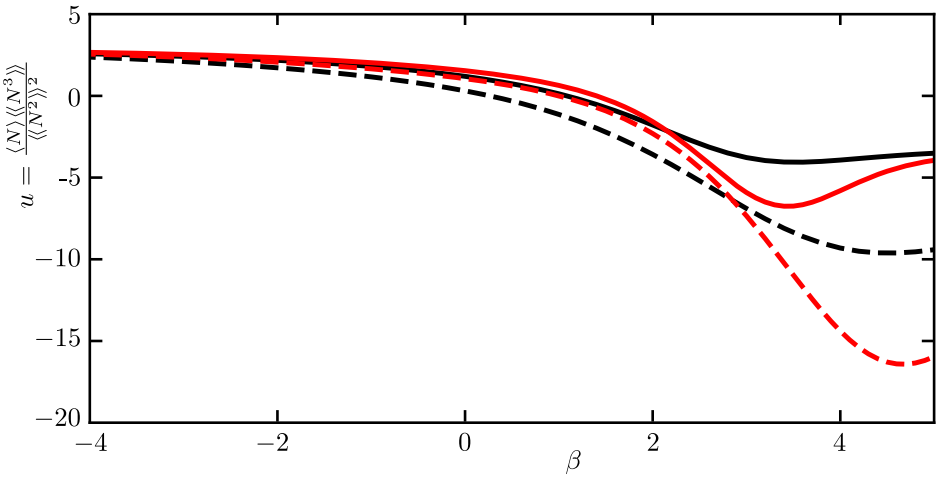

Figure 5.6: Universal ratio for the non-degenerate (black) and degenerate (red) parametric oscillator for the exponents $m = 2(4)$ in solid (dashed) lines. Below threshold, the universal ratio starts at the value $u = 3$ and slowly starts to decrease and also assumes a negative value. For larger driving, the universal ratio should converge to the value $u = 1$ due to the Poissonian statistics. Therefore, u starts to increase again and shows non-monotonous behavior.

cumulant. After it drops far below 0, it starts to rise again for increasing β since the classical regime, where $u = 1$, is approached. At threshold, the universal ratio assumes $u = 1.195\,(0.308)$ for $m = 2(4)$ and $u = 1.543\,(1.054)$ for $m = 2(4)$ for the non-degenerate and degenerate case respectively.

Chapter 6

Conclusion and outlook

This thesis has dealt with bosonic driven-dissipative systems that are described by a Lindblad master equation, compactly expressed by a Liouvillian $\mathcal{L}$. In Ch. 2, we have shown how to solve a quadratic Liouvillian to obtain the spectrum and the time evolution. To this end, we have proven a theorem about the diagonalization of a complex symmetric matrix using a symplectic transformation. By introducing a superoperator formalism, we have mapped the task of diagonalizing the Liouvillian to this problem. There, the complex symmetric matrix represents the Liouvillian while the symplectic form encodes the bosonic structure. We have shown that non-Hermitian Hamiltonians naturally appear in our approach and that noise does not influence the spectrum. It has been pointed out that the trace preservation is the key ingredient to diagonalize the Liouvillian, the eigenstates, and therefore the spectrum. It also provides a distinguished left eigenstate with the eigenvalue $\lambda = 0$ which in turn allows the identification of a right eigenstate with the same eigenvalue. This right eigenstate plays the important role of the stationary state. Furthermore, the case of non-diagonalizable Liouvillians have been discussed. In this case Jordan blocks appear which alters the time evolution and leads to a non-exponential time evolution. We have provided an explicit expression of the time evolution operator for the case of a single boson. But the procedure can be generalized for systems of multiple bosons and possibly larger Jordan blocks. The approach using a symplectic transformation has also been proven useful when counting fields are included. Then, the trace preservation is lost and previous approaches to diagonalize the Liouvillian are not possible anymore. Our method however is able obtain the generating function in the limit of long measurement times. The generating function can be then used to obtain the cumulants of observables. In Ch. 4 and 5, this has been used to obtain the radiation statistics of the degenerate and non-degenerate parametric oscillator.

How symmetries are included in the formalism of Ch. 2 has been the topic of Ch. 3. We have started with the hermiticity of the density matrix. It is not a symmetry in the conventional sense but provides a useful tool for the diagonalization of the Liouvillian. The hermiticity also explains the fact that the eigenvalues of the Liouvillian are either real or appear in complex conjugate

pairs. Additionally, it puts constraints on the Liouvillian itself, on observables, and on conventional symmetries. Afterwards, it has been shown how unitary symmetries of the Hamiltonian can be elevated to a symmetry of the Liouvillian. It has been pointed out that due to the hermiticity constraint, unitary and anti-unitary symmetries are equivalent. Then the case of $\mathcal{PT}$-'symmetry' has been discussed. It describes systems with balanced gain and loss. This balancing is expressed by an exchange of creation and annihilation operators. For both symmetries we have provided the most general form of the symmetry matrix and properties that the individual parts of the Liouvillian have to fulfill.

In Ch. 4, we have applied the methods introduced in Ch. 2 to the case of the degenerate parametric oscillator. The diagonalization has made the identification of two different timescales possible. The long-time dynamics predicts an instability when the driving strength exceeds the damping. In the critical regime around the instability nonlinearities have to be taken into account which stabilize the system. This limits analytical insight. But the identification of a slow and fast timescale make the derivation of an effective universal Liouvillian possible. It describes the relevant slow dynamics and enables further analysis. By comparing the resulting photon counting statistics to the full system, we have shown that the universal Liouvillian provides a good description of the system.

In Ch. 5, we have studied the non-degenerate parametric oscillator where two oscillators are driven at the sum of their resonance frequencies. Again, the diagonalization makes the identification of a fast and slow timescale possible with diverging dynamics above a certain threshold. Employing the methods of Ch.4, we have derived an effective model of the slow dynamics. Additionally, it has been assumed that one of the oscillator is heavily damped. This makes phase-insensitive amplification in the other oscillator possible. This fact is expressed in the Liouvillian of the effective model. It resembles a 2D-Fokker-Planck equation which is a two-dimensional coupled partial differential equation. We make use of the rotational invariance of the Liouvillian to obtain a one-dimensional differential equation. This has been further transformed into a simple eigenvalue problem. This makes the efficient evaluation of the Liouvillian possible. Finally, we have determined the radiation statistics of the non-degenerate parametric oscillator. This has been compared to the degenerate case, where similarities and differences have been pointed out. The statistics align also with the classical expectation above threshold.

This work provides a good starting point for further research on interesting questions. For example, the diagonalization can be used to analyze how a non-resonant drive impacts the dynamics as well as radiation statistics. Also, the universal Liouvillians in this work have been derived for small nonlinearities, $\alpha \ll 1$. The study of larger nonlinearities, $\alpha \approx 1$, remains as an open research topic. Further, an investigation of the radiation statistics for higher order parametric resonances would be interesting. Moreover, the discussion about symmetries of the Lindblad equation enables the study of symmetry breaking in

open quantum systems. It is also interesting to see whether the inclusion of source terms can reveal new symmetries.

Appendix A

Diagonalization for the non-degenerate parametric oscillator

In this appendix, we show the details about the diagonalization of the Lindblad equation given by the Hamiltonian in Eq. (5.5) and by the jump operators in (5.6). For clarity, we also show them here:

$$\begin{aligned} H &= \frac{i\epsilon}{2}\left(ab - a^\dagger b^\dagger\right), \\ \mathcal{J}_{1,k} &= \sqrt{\gamma_k(\bar{n}_k+1)}k, \\ \mathcal{J}_{2,k} &= \sqrt{\gamma_k \bar{n}_k}\, k^\dagger, \end{aligned} \tag{A.1}$$

with $k = a, b$. The relevant matrices to construct the blocks of L in Eq. (2.19) are given by

$$\Delta = \frac{i\epsilon}{2}\begin{pmatrix} 0 & 1 \\ 1 & 0 \end{pmatrix}, \quad V = \begin{pmatrix} \gamma_a(\bar{n}_a+1) & 0 \\ 0 & \gamma_b(\bar{n}_b+1) \end{pmatrix}, \quad W = \begin{pmatrix} \gamma_a\bar{n}_a & 0 \\ 0 & \gamma_b\bar{n}_b \end{pmatrix}. \tag{A.2}$$

The eigenvalues of the corresponding Liouvillian are given by

$$\lambda_s = -\frac{1}{4}\left(\gamma_a + \gamma_b - \sqrt{4\epsilon^2 + (\gamma_a - \gamma_b)^2}\right), \tag{A.3}$$

$$\lambda_f = -\frac{1}{4}\left(\gamma_a + \gamma_b + \sqrt{4\epsilon^2 + (\gamma_a - \gamma_b)^2}\right), \tag{A.4}$$

with double degenerate eigenvalues but diagonalizable Liouvillian. The diagonalized form then reads

$$\mathcal{L} = \lambda_s(v_{s,1}u_{s,1} + v_{s,2}u_{s,2}) + \lambda_f(v_{f,1}u_{f,1} + v_{f,2}u_{f,2}). \tag{A.5}$$

The most general form of the new ladder operators is quite complicated and does not provide any insights. Since we are interested in the critical regime close to threshold, we put $\epsilon = \sqrt{\gamma_a\gamma_b}$ where it is applicable. This results in

$\lambda_f \approx -(\gamma_a + \gamma_b)/2$ while we let λ_s unchanged. For the creation operators at threshold, we obtain

$$\begin{aligned} v_{s,1} &= a_q + \sqrt{\frac{\gamma_a}{\gamma_b}}\, b_q^\dagger, \quad v_{s,2} = a_q^\dagger + \sqrt{\frac{\gamma_a}{\gamma_b}}\, b_q, \\ v_{f,1} &= b_q - \sqrt{\frac{\gamma_a}{\gamma_b}}\, a_q^\dagger, \quad v_{f,2} = b_q^\dagger - \sqrt{\frac{\gamma_a}{\gamma_b}}\, a_q. \end{aligned} \tag{A.6}$$

We see that they are a linear combination of the 'q'-operators as expected from the trace preservation pointed out in Sec. 2.2.2. The annihilation operators read

$$\begin{aligned} u_{s,1} &= -\Gamma_b a_c^\dagger + \Gamma_* b_c - \Gamma_*^2 \frac{\bar{n}\sqrt{\gamma_a\gamma_b}}{4\lambda_s}\, b_q - \Gamma_*^2 \frac{\bar{n}\sqrt{\gamma_a\gamma_b}}{4\lambda_s}\, a_q^\dagger, \\ u_{s,2} &= \Gamma_b a_c - \Gamma_* b_c^\dagger - \Gamma_*^2 \frac{\bar{n}\sqrt{\gamma_a\gamma_b}}{4\lambda_s}\, b_q^\dagger - \Gamma *^2 \frac{\bar{n}\sqrt{\gamma_a\gamma_b}}{4\lambda_s}\, a_q, \\ u_{f,1} &= -\Gamma_b b_c^\dagger - \Gamma_* a_c - \Gamma_*^3 \frac{\bar{n}}{2}\, a_q - \Gamma_*^3 \frac{\bar{n}}{2}\, b_q^\dagger, \\ u_{f,2} &= \Gamma_b b_c + \Gamma_* a_c^\dagger - \Gamma_*^3 \frac{\bar{n}}{2}\, a_q^\dagger - \Gamma_*^3 \frac{\bar{n}}{2}\, b_q, \end{aligned} \tag{A.7}$$

where we have used the abbreviations $\Gamma_b = \gamma_b/(\gamma_a + \gamma_b)$, $\Gamma_* = \sqrt{\gamma_a\gamma_b}/(\gamma_a + \gamma_b)$, and $\bar{n} = (1 + \bar{n}_a + \bar{n}_b)/2$. When we further assume that $\gamma_b \gg \gamma_a$, then $\Gamma_b \approx 1$ and $\Gamma_* \approx \sqrt{\gamma_a/\gamma_b}$.

Bibliography

[1] Ling-An Wu, H. J. Kimble, J. L. Hall, and Huifa Wu. Generation of Squeezed States by Parametric Down Conversion. *Phys. Rev. Lett.*, 57:2520–2523, Nov 1986.

[2] A. Peugeot, G. Ménard, S. Dambach, M. Westig, B. Kubala, Y. Mukharsky, C. Altimiras, P. Joyez, D. Vion, P. Roche, D. Esteve, P. Milman, J. Leppäkangas, G. Johansson, M. Hofheinz, J. Ankerhold, and F. Portier. Generating Two Continuous Entangled Microwave Beams Using a dc-Biased Josephson Junction. *Phys. Rev. X*, 11:031008, Jul 2021.

[3] Peter Kirton, Mor M. Roses, Jonathan Keeling, and Emanuele G. Dalla Torre. Introduction to the Dicke Model: From Equilibrium to Nonequilibrium, and Vice Versa. *Advanced Quantum Technologies*, 2(1-2):1800043, 2019.

[4] Markus Aspelmeyer, Tobias J. Kippenberg, and Florian Marquardt. Cavity optomechanics. *Rev. Mod. Phys.*, 86:1391–1452, Dec 2014.

[5] L. Arndt and F. Hassler. Universality of photon counting below a local bifurcation threshold. *Phys. Rev. A*, 103:023506, 2021.

[6] F. Hassler, S. Kim, and L. Arndt. Radiation statistics of a degenerate parametric oscillator at threshold. *arXiv:2208.14886*, 2023.

[7] F. Minganti, A. Biella, N. Bartolo, and C. Ciuti. Spectral theory of Liouvillians for dissipative phase transitions. *Phys. Rev. A*, 98:042118, 2018.

[8] T. Prosen. Third quantization: a general method to solve master equations for quadratic open Fermi systems. *New J. Phys.*, 10:043026, 2008.

[9] T. Prosen and T. H. Seligman. Quantization over boson operator spaces. *J. Phys. A*, 43:392004, 2010.

[10] C. Guo and D. Poletti. Solutions for bosonic and fermionic dissipative quadratic open systems. *Phys. Rev. A*, 95:052107, 2017.

[11] A. McDonald and A. A. Clerk. Exact Solutions of Interacting Dissipative Systems via Weak Symmetries. *Phys. Rev. Lett.*, 128:033602, 2022.

[12] F. Thompson and A. Kamenev. Field Theory of Many-Body Lindbladian Dynamics. *arXiv:2301.02953*, 2023.

[13] A. McDonald and A. A. Clerk. Third quantization of open quantum systems: new dissipative symmetries and connections to phase-space and Keldysh field theory formulations. *arXiv:2302.14047*, 2023.

[14] S. Kim and F. Hassler. Third quantization for bosons: symplectic diagonalization, non-Hermitian Hamiltonian, and symmetries. *arXiv:2304.02367*, 2023.

[15] F. R. Gantmacher. *Theory of Matrices.* Chelsea Publishing Company, Vol. 1, Ch. V, §1, 1959.

[16] A. J. Laub and K. Meyer. Canonical forms for symplectic and Hamiltonian matrices. *Celest. Mech. Dyn. Astron.*, 9:213, 1974. See in particular corrolary 3.1.

[17] F. Nicacio. Williamson theorem in classical, quantum, and statistical physics. *Am. J. Phys.*, 89:1139–1151, 2021.

[18] A. Kamenev. *Field Theory of Non-Equilibrium Systems.* Cambridge University Press, 2011.

[19] J. H. P. Colpa. Diagonalization of the quadratic boson hamiltonian. *Physica A*, 93:327–353, 1978.

[20] E. J. Bergholtz, J. C. Budich, and F. K. Kunst. Exceptional topology of non-hermitian systems. *Rev. Mod. Phys.*, 93:015005, 2021.

[21] F. Brange, P. Menczel, and C. Flindt. Photon counting statistics of a microwave cavity. *Phys. Rev. B*, 99:085418, 2019.

[22] C. W. J. Beenakker. Thermal radiation and amplified spontaneous emission from a random medium. *Phys. Rev. Lett.*, 81:1829, 1998.

[23] Dania Kambly, Christian Flindt, and Markus Büttiker. Factorial cumulants reveal interactions in counting statistics. *Phys. Rev. B*, 83:075432, 2011.

[24] V. V. Albert and L. Jiang. Symmetries and conserved quantities in Lindblad master equations. *Phys. Rev. A*, 89:022118, 2014.

[25] B. Buča and T. Prosen. A note on symmetry reductions of the Lindblad equation: transport in constrained open spin chains. *New J. Phys.*, 14:073007, 2012.

[26] C. M. Bender, S. Boettcher, and P. N. Meisinger. $\mathcal{PT}$-symmetric quantum mechanics. *J. Math. Phys*, 40:2201, 1999.

[27] Y. Nakanishi and T. Sasamoto. $\mathcal{PT}$ phase transition in open quantum systems with Lindblad dynamics. *Phys. Rev. A*, 105:022219, 2022.

[28] J. Huber, P. Kirton, S. Rotter, and P. Rabl. Emergence of $\mathcal{PT}$-symmetry breaking in open quantum systems. *SciPost Phys.*, 9:052, 2020.

[29] F. Roccati, S. Lorenzo, G. M. Palma, G. T. Landi, M. Brunelli, and F. Ciccarello. Quantum correlations in $\mathcal{PT}$-symmetric systems. *Quantum Sci. Technol.*, 6:025005, 2021.

[30] C. Padurariu, F. Hassler, and Yu. V. Nazarov. Statistics of radiation at Josephson parametric resonance. *Phys. Rev. B*, 86:054514, 2012.

[31] G. C. Ménard, A. Peugeot, C. Padurariu, C. Rolland, B. Kubala, Y. Mukharsky, Z. Iftikhar, C. Altimiras, P. Roche, H. le Sueur, P. Joyez, D. Vion, D. Esteve, J. Ankerhold, and F. Portier. Emission of Photon Multiplets by a dc-Biased Superconducting Circuit. *Phys. Rev. X*, 12:021006, Apr 2022.

[32] S. Kim. *Single Mode Lindblad Description of the Parametric Instability.* B.Sc. thesis, RWTH Aachen University, 2021.

[33] C. W. Gardiner. *Handbook of Stochastic Methods.* Springer-Verlag, Berlin, 3$^{\text{rd}}$ edition, 2004.

[34] W. Wustmann and V. Shumeiko. Nondegenerate Parametric Resonance in a Tunable Superconducting Cavity. *Phys. Rev. Appl.*, 8:024018, Aug 2017.

[35] G. Szegö. *Theory of Matrices.* American Mathematical Society colloquium publications, Vol. 23, Ch. V, §100, 1939.

[36] M. Abramowitz and I. A. Stegun. *Handbook of Mathematical Functions with Formulas, Graphs, and Mathematical Tables.* New York: Dover, pp. 446-452, Cambridge, 9$^{\text{th}}$ edition, 1972.

[37] W. N. Bailey. *Generalised Hypergeometric Series.* Cambridge University Press, Cambridge, 1935.

Acknowledgements

First of all, I want to thank Fabian Hassler for making this thesis possible. His guidance has not only deepened my understanding of the subject but also my enthusiasm for physics. Although I may have found some of his words puzzling at times, I have always gained valuable knowledge and insights from our conversations.

I also want to thank Markus Müller for being my second examiner.

I would like to express my appreciation to Lisa Arndt for introducing me to this topic and sparking my interest in it.

In addition, I am thankful for all the people at the IQI for the nice environment at the office. Especially Alexander Ziesen, David Scheer, and Evangelos Varvelis for the fun evenings after the group meetings.

Furthermore, I am grateful for my partner Hannah-Lea and my brother for proofreading my work. I want to thank them and my mother for their love and support.